Spring 2023

Dendrohydrological Reconstruction of North Fork Nooksack River August Streamflow from Subannual Mountain Hemlock Ring-Widths, Cascade Mountains, Washington State

Hannah LaGassey
Western Washington University, hrlagassey@gmail.com

Dendrohydrological Reconstruction of North Fork Nooksack River August Streamflow from Subannual Mountain Hemlock Ring-Widths, Cascade Mountains, Washington State

By

Hannah LaGassey

Accepted in Partial Completion
of the Requirements for the Degree
Master of Arts

ADVISORY COMMITTEE

Dr. Aquila Flower, Chair

Dr. Andrew Bunn

Dr. Robert Mitchell

GRADUATE SCHOOL

David L. Patrick, Dean

Master's Thesis

In presenting this thesis in partial fulfillment of the requirements for a master's degree at Western Washington University, I grant to Western Washington University the non-exclusive royalty-free right to archive, reproduce, distribute, and display the thesis in any and all forms, including electronic format, via any digital library mechanisms maintained by WWU.

I represent and warrant this is my original work, and does not infringe or violate any rights of others. I warrant that I have obtained written permissions from the owner of any third party copyrighted material included in these files.

I acknowledge that I retain ownership rights to the copyright of this work, including but not limited to the right to use all or part of this work in future works, such as articles or books.

Library users are granted permission for individual, research and non-commercial reproduction of this work for educational purposes only. Any further digital posting of this document requires specific permission from the author.

Any copying or publication of this thesis for commercial purposes, or for financial gain, is not allowed without my written permission.

Hannah LaGassey
January 1, 2023

Dendrohydrological Reconstruction of North Fork Nooksack River August Streamflow from Subannual Mountain Hemlock Ring-Widths, Cascade Mountains, Washington State

A Thesis
Presented to
The Faculty of
Western Washington University

In Partial Fulfillment
Of the Requirements for the Degree
Master of Arts

By
Hannah LaGassey
January, 2023

Abstract

Climate warming is driving changes to snowpack and streamflows in snow and ice-driven systems throughout the world. To better understand present and future conditions, we need to examine conditions prior to the onset of climate warming. Tree ring records are used widely to reconstruct pre-instrumental climate and hydrological records. Some locations are more conducive to this methodology than others, however, and moisture-rich environments such as the west slopes of the Cascade mountains continue to present challenges to effective hydrological record reconstruction. Previous researchers working in this environment have employed several techniques in response to this problem, which require integrated dendrochronological and hydrological modeling, independently reconstructed climate records, or access to an X-ray densiometer. We advocate for the use of a less costly technique in terms of skill, data, and money that can be used alone or in tandem with more advanced techniques to improve the quality of hydrological reconstruction models in this environment: subannual ring-width measurements. As of yet, no one has applied this technique to the species mountain hemlock (*Tsuga mertensiana*), or to streamflow reconstruction modeling in the coastal Pacific Northwest. We found that separating annual ring-widths into subannual earlywood and adjusted latewood measurements resulted in stronger and less confounded associations with climate and hydrological data, and significantly improved the skill of a streamflow reconstruction model of average August streamflow of the upper North Fork Nooksack River in northern Washington State, USA. Earlywood associated most strongly with winter through summer snowpack of the same water year, and adjusted latewood associated most strongly with late summer temperature and precipitation of the same and previous water year. Earlywood contained a streamflow signal from the same water year and adjusted latewood contained a streamflow signal from the previous

water year, allowing for the development of a streamflow reconstruction model. We observed an improvement in reconstruction model fit of 7% using earlywood and forward-lagged adjusted latewood rather than annual ring-width.

Note that for publication purposes, I chose to use first-person plural rather than singular throughout the text because there will be multiple authors on the final manuscript submitted for publication.

Table of Contents

List of Tables

List of Figures

1.0 Introduction

Snowpack and streamflows in snow and ice-driven systems across the world are experiencing dramatic changes in response to a warming climate. Across western North America, more than 98% of snow measurement stations with more than 40 years of recorded data have experienced reductions in April 1st SWE (snow water equivalent) (Musselman et al, 2021). Snowpack in the North Cascades decreased by an estimated 25% from 1950-2006 (Mote et al, 2008). Glaciers on Mount Baker lost an estimated 12-20% of their volume from 1990-2010 (Pelto & Brown, 2012). As climate warming continues, declining snowpack and glacial ice will lead to streamflow droughts during late summer in the transient snow-rain watersheds on the west slopes of the Cascade mountains. This is particularly concerning in the Pacific Northwest region, where summer precipitation is low but human demands on summer water resources are high (Hamlet et al, 2005; Mote et al, 2005; Dudley et al, 2016; Mote et al, 2018; Dierauer et al, 2019). Unfortunately, little is understood about pre-instrumental trends and variability in late summer streamflow on the west slopes of the Cascades. Increasing our understanding of past late summer streamflow characteristics can provide context for future conditions under climate change.

Streamflows in the Cascade mountains are highly responsive to climate fluctuations. This region contains an abundance of watersheds with large areal proportions near or above snowline elevation. Changes in the ratio of precipitation falling as rain or snow in these watersheds can cause significant changes in streamflow volume and timing throughout the year (Leung & Wigmosta, 1999; Hamlet et al, 2005; Li et al, 2017; Mote et al, 2018). Instrumental streamflow records show changes in streamflow regimes corresponding to human-induced climate change, with snow melting earlier in the warm season and snowpack accumulation starting later in the

cold season (Mote et al, 2005; Stewart et al, 2005; Mote et al, 2018; Musselman et al, 2021). This causes decreased water storage on the land and decreased streamflow in late summer when precipitation is scarce and the snowpack has melted (Barnett et al, 2005; Hamlet et al, 2007; Luce & Holden, 2009; Tohver et al, 2014; Vano et al, 2015; Dudley et al, 2016; Li et al, 2017). In watersheds containing glaciers, late summer streamflow is regulated by glacial melt (Fountain & Tangborn, 1985; Granshaw & Fountain, 2006; Moore et al, 2009; Pelto, 2015). However, as glaciers shrink in response to climate change they contribute decreasing volumes of meltwater to streamflow (Stahl et al, 2006; Stahl & Moore, 2006; Moore et al, 2009; Murphy, 2016).

Streams flowing from the Cascade mountains supply the growing human populations of Washington State, Oregon, northern California, and southwestern British Columbia with water resources. These streams are also home to ecologically and culturally important animal species such as anadromous fish that are negatively affected by decreasing flows and rising stream temperatures (Mantua et al, 2010; Isaak et al, 2011). Water resource planners raise concerns about future water availability in late summer under the effects of climate change (Bach, 2002; Payne et al, 2004; Barnett et al, 2005; Wiley & Palmer, 2008; Grah & Beaulieu, 2013; Dickerson-Lange & Mitchell, 2014; Murphy, 2016; Li et al, 2017). However, our ability to study those water resources is limited by the length of our data records. Instrumental streamflow records in the Cascade mountains typically begin in the first half of the twentieth century, well after the onset of human-induced climate change (Abram et al, 2016). In order to provide better context for present and future conditions, pre-instrumental records are required.

One method of acquiring pre-instrumental records involves using the annual ring-widths of climate-limited trees as a proxy for past climate and hydrological conditions (Fritts, 1976; Cook & Kairiukstis, 1990). The reconstruction of streamflow records in moisture-limited

environments has been done with great success in western North America (Watson & Luckman, 2005; Woodhouse et al, 2006). However, in contrast to the majority of western North America, tree growth on the west slopes of the Cascades is not strongly limited by moisture (Marcinkowski et al, 2015; Trinies, 2019). This makes the reconstruction of streamflow records in this environment difficult (Mood & Smith, 2021). Though the reconstruction of rain-dominated streamflows in the region has thus far eluded researchers, some have successfully reconstructed snow-dominated and transient snow-rain summer streamflows with trees growing in places where snowpack limits growing season length (Hart et al, 2010; Starheim et al, 2013; Coulthard & Smith, 2016; Mood & Smith, 2021).

This study seeks to reconstruct the average August streamflow record of the upper North Fork Nooksack River, where snowpack and glacial melt drive late summer streamflow (Bach, 2002; Dickerson-Lange & Mitchell, 2014; Murphy, 2016). We do so using subannual tree ring-width measurements, a method not yet applied to streamflow reconstruction on the west slopes of the Cascade mountains.

1.1 Research Background

Tree-ring records have been used to reconstruct streamflow records throughout western North America, providing streamflow information from centuries prior to human-induced climate change (Meko et al, 2001; Watson & Luckman, 2005; Woodhouse et al, 2006). At high elevations on the west slopes of the Cascade mountains, the growth of trees tends to be limited by deep, persistent snowpack (Peterson & Peterson, 1994; Peterson & Peterson, 2001; Peterson et al, 2002; Ettinger et al, 2011). The radial growth of mountain hemlock (*Tsuga mertensiana*) is particularly sensitive to fluctuations in snowpack via length of growing season (Brubaker, 1980;

Heikkinen, 1985; Graumlich & Brubaker, 1986; Woodward et al, 1994; Smith & Larocque, 1998; Gedalof & Smith, 2001; Peterson & Peterson, 2001). This relationship between mountain hemlock growth and snowpack not only makes snowpack reconstruction possible (Appleton & St. George, 2018; Harley et al, 2020; Mood et al, 2020; Coulthard et al, 2021), it also makes the reconstruction of snow-dominated streamflows possible (Gedalof et al, 2004; Hart et al, 2010; Lutz et al, 2012; Starheim et al, 2013; Littell et al, 2016; Coulthard & Smith, 2016; Mood & Smith, 2021).

Prior streamflow reconstructions in the Pacific Northwest region have been located in the Columbia River basin (Gedalof et al, 2004; Lutz et al, 2012; Littell et al, 2016), on Vancouver Island (Coulthard & Smith, 2016), or in the Coast Mountains and Cascades of southwestern British Columbia, Canada (Hart et al, 2010; Starheim et al, 2013; Mood & Smith, 2021). This study seeks to provide a streamflow reconstruction located on the west slopes of the Cascade mountains in northern Washington State, U.S.A., for the upper North Fork Nooksack River. No significant diversion structures have been placed on this stream, so measured streamflow values represent natural flows (Bach, 2002).

Furthermore, this study seeks to follow Lutz et al (2012), Starheim et al (2013), Coulthard & Smith (2016), Coulthard et al (2016), and Mood & Smith (2021) in focusing on late summer streamflow due to the stress on water resources projected to occur in response to climate change. Additionally, dendrohydrological reconstructions in the wet coastal Pacific Northwest environment are currently restricted to seasons when snow and glacier melt dominate flow regimes, such as late summer, since tree growth west of the Cascade crest is not strongly limited by moisture (Marcinkowski et al, 2015; Trinies, 2019; Mood & Smith, 2021).

The North Fork Nooksack basin contains glaciers on the north flanks of Mt Baker and Mt Shuksan, representing 77% of the total glaciated area within the main stem Nooksack basin. The Middle Fork basin contains the remaining 23% of glaciated area and the South Fork 0% (Truitt, 2018). Loss of glaciers in response to climate change could significantly reduce late summer streamflow. Dickerson-Lange & Mitchell (2014) forecasted a possible 21-33% reduction in main stem summer streamflows by the 2050s. Within the North Fork basin alone, Murphy (2016) predicted a decrease in late summer streamflows of 62-77% by 2075, with glacial meltwater contributing half the amount of 2025 volumes.

Increasing human demands on local water resources, warming temperatures, and the melting of snowpack and glaciers indicate the necessity of studying North Fork Nooksack River flow dynamics (Grah & Beaulieu, 2013). This study seeks to contribute to the understanding of the pre-instrumental upper North Fork Nooksack River system by reconstructing its average August streamflow over the past four centuries.

In response to the difficulties of reconstructing hydrological variables using tree rings in a moisture-rich environment, dendrochronologists have employed a number of advanced techniques aimed at improving the hydrological signals extracted from tree-rings. Lutz et al (2012) used an integrated modeling approach by reconstructing cool season precipitation from annual tree ring-width data and used this to develop meteorological forcings used in the Variable Infiltration Capacity (VIC) hydrological model to produce a warm season streamflow reconstruction. Coulthard et al (2016) used annual tree ring-width data in tandem with reconstructed Palmer Drought Severity Index (PDSI) data produced from independent tree-ring samples as predictors of summer streamflow. In a similar fashion, Mood & Smith (2021) used annual tree ring-width data in tandem with independently-reconstructed Pacific Decadal

Oscillation (PDO) data as predictors of July-August streamflow. Starheim et al (2013) used annual tree ring-width and maximum density data as predictors of July-August streamflow. These studies all explained a greater amount of variance in streamflow in reconstruction models than they would have with annual tree ring-width predictors alone. However, the success of their methods relied on specialized skills with hydrological modeling, the prior existence of independently-developed PDSI or PDO reconstructions or the time and resources to create said reconstructions in addition to a streamflow reconstruction, and access to an expensive X-ray densiometer, respectively.

This study explores the use of a less costly technique in terms of skill, time, and monetary investment to increase the strength of hydrological signals derived from tree rings: subannual earlywood and latewood ring-width measurements. Earlywood is the lighter portion of annual tree-rings, with larger cells and thinner cell walls, and represents early season radial growth. Latewood is the darker portion of annual tree-rings, with smaller cells and thicker cell walls, and represents late season radial growth. These anatomically distinct features can be identified visually and measured with the same tools that most tree-ring researchers already possess, such as a Velmex system and ring-width measurement software such as the free Tellervo software (Speer, 2010; Brewer, 2014).

In climate-limited environments, trees may react to different climate variables throughout their growing season (Fritts, 1976). The utility of subannual ring-width measurements of Douglas-fir (*Pseudotsuga menziesii*) and Ponderosa pine (*Pinus ponderosa*) in climate reconstruction models has been demonstrated successfully in the American Rockies (Crawford et al, 2015) and in the desert southwest (Meko & Baisan, 2001; Stahle et al, 2009; Griffin et al, 2011), where earlywood ring-widths correlate with cool season precipitation and latewood ring-

widths correlate with warm season precipitation. These studies all statistically correct for the dependence of latewood on antecedent earlywood growth at the site or core level by modeling latewood width (dependent variable) as a function of earlywood width (independent variable) and taking the residuals + 1 as adjusted latewood width. In this manner, correlation between earlywood and adjusted latewood is removed and these subannual ring-width measurements represent separate growth signals within the same growing season.

To the best of our knowledge, no one has yet applied this technique to mountain hemlock or to streamflow reconstruction in the coastal Pacific Northwest. This paper addresses the following research questions:

1. How do subannual ring-width measurements in mountain hemlock associate with climate and hydrology variables at high elevation in the North Cascades?
2. Can subannual ring-width measurements be used to produce a reliable reconstruction of late summer streamflow in the coastal Pacific Northwest?

2.0 Methods

2.1 Study Area

The North Fork Nooksack basin is located on the north sides of Mt Baker and Mt Shuksan, adjacent the US-Canada border in the Cascade mountains of Washington State, U.S.A. The North Fork Nooksack River captures runoff from 760 square kilometers of basin area above the confluence with the Middle Fork Nooksack near Welcome, Washington. Our study area encompasses the upper 269 square kilometers of the North Fork Nooksack basin, spanning an

elevation of 390 meters (1,280 feet) near Glacier, WA to 3,286 meters (10,781 feet) at the summit of Mt Baker. The upper basin contains montane forest, subalpine parkland, and glaciated terrain. Our study sites sit within the upper basin or near the basin boundary (Figure 1). The upper basin lies in the transition zone between the "Warm Summer Mediterranean" and "Temperate Oceanic" Köppen Climate Classification zones (Peel et al, 2007). About 70% of the region's precipitation falls between October and March (Dickerson-Lange & Mitchell, 2014). A large proportion of winter precipitation in the upper basin falls as snow and is stored on the landscape for six or more months of the year until it is melted in spring and summer when warm and dry conditions prevail (Figure 2). This basin was selected due to existing tree core samples collected by A.G. Bunn at the Heather Meadows site within the basin (Bunn, 2012).

Snowpack and glacier melt drive the streamflow regime of the North Fork Nooksack River (Bach, 2002; Dickerson-Lange & Mitchell, 2014; Pelto, 2015; Murphy, 2016). The highest flows occur in early summer corresponding to warm temperatures and subsequent melt/runoff, and the lowest flows occur in late winter corresponding to cold temperatures and snowpack accumulation/storage (Figure 3).

2.2 Tree-Ring Data

At climatologically extreme range limits, the radial growth of trees is primarily a function of climate conditions (Fritts, 1976; Ettinger et al, 2011). Our study sites were located at the climatological range limit of mountain hemlock trees corresponding to persistent snowpack. All three study sites sit on north-facing slopes in high elevation (4,350 to 4,900 feet), open-canopy parkland environments near treeline at Heather Meadows, Grouse Ridge, and Canyon Ridge

(Figure 1). The Heather Meadows site included cores collected by this study and cores previously collected by A.G. Bunn (2012).

In the summer of 2019, we cored 18 trees at Heather Meadows (in addition to the 14 trees previously cored by A.G. Bunn), 20 trees at Grouse Ridge, and 20 trees at Canyon Ridge. We took at least two cores per tree at breast height using a 3mm Haglof increment borer. We cored parallel to the slope in order to minimize the inclusion of reactive growth caused by geomorphic processes or other physical damage. Coordinate location and diameter at breast height were recorded for each sample tree. Selected sample trees had minimal visible structural damage and produced cores without rot. Cores were transported to the lab in paper straws within a protective case.

We placed cores in a drying oven at 40 degrees Celsius for 24 hours due to the high humidity of ambient air. Cores were then mounted on permanent fiberboard holders with Elmer's wood glue. Once dry, cores were sanded to a polish with a series of progressively finer-graded sandpaper up to 600-grit to reveal ring boundaries visible at the cellular level under magnification. We estimated sample ages using the dotting method (Stokes & Smiley, 1968). We measured ring widths, separated into earlywood and latewood, under a dissecting microscope with a Velmex unislide and Tellervo software (Speer, 2010; Brewer, 2014).

After visual crossdating, we statistically crossdated sample total ring-widths using individual series from all three study sites. We used COFECHA software to verify the specific year each tree-ring formed (Holmes, 1983). Series which did not express a unified regional signal were removed prior to further analyses. We altered earlywood and latewood ring dates to match corresponding annual ring dates. The overall sample period spanned 1430-2018.

We detrended individual ring-width series with a 100-year spline to remove age-related growth trends and preserve most low-frequency variability in ring-widths using R package dplR (Fritts, 1976; Bunn, 2008). We calculated prewhitened residual ring-width chronologies of total ring-width, earlywood width, and latewood width using a bi-weight robust mean to correct for biologically driven, low-order autocorrelation and limit the influence of outlier values (Cook & Kairiukstis, 1990). We trimmed chronologies to an appropriate sample depth using a Subsample Signal Strength (SSS) cutoff of 0.85 (Buras, 2017).

To correct for the influence of antecedent earlywood growth on latewood growth, we calculated adjusted latewood chronologies at the site level after Meko & Baisan (2001) and Stahle et al (2009). For each study site, we made a linear model with the site latewood width chronology as the dependent variable and the site earlywood width chronology as the independent variable, taking the residuals as the site adjusted latewood chronology. The three site adjusted latewood chronologies averaged together made up the regional adjusted latewood chronology.

$$LWa = \text{residuals (linear model } (LW \sim EW)) + 1$$

Where:

LWa = adjusted latewood chronology

LW = raw latewood chronology (dependent variable)

EW = earlywood chronology (independent variable)

To further reduce statistical noise and amplify unified regional signals in our tree-ring data, we also extracted principal components from the ring-width chronologies (Peters et al,

1981). Variables were centered and scaled in R using the 'prcomp' function (R Core Team, 2022). We ran separate principal component analyses for each annual and subannual tree-ring variable (total ring-width, earlywood, raw latewood, and adjusted latewood), where inputs were the corresponding site ring-width chronologies. The results were four principal component (PC) chronologies consisting of unitless tree-ring proxies (eigenvalues). We examined the amount of variance explained by the principal components of each tree-ring variable, taking only the first principal component of each for further analyses. In the case of all variables, principal components after the first explained considerably smaller proportions of variance in ring-width (=< 21%) (Table 1).

2.3 Hydrology & Climate Data

Monthly average streamflow data from 1938-2018 came from USGS stream gauge no.12205000, "NF Nooksack River below Cascade Creek near Glacier, WA" (USGS, 2019).

Monthly snowpack data from January 1950 to February 2012 came from Hostetler and Alder, 2016. Snowpack data were simulated with a Monthly Water Balance Model (MWBM) using 800m Parameter-elevation Regression on Independent Slopes Model (PRISM) data as model inputs over the conterminous US (PRISM, 2014). The model calculated monthly snow water equivalent (SWE) values based on monthly total precipitation and monthly average temperature. Modeled data were examined for error with observed data from the Snow Data Assimilation System (SNOWDAS) and the Snowpack Telemetry Network (SNOTEL) (Hostetler & Alder, 2016; Alder & Hostetler, 2018). We ran a comparison of modeled and observed SWE data at the three nearest SNOTEL sites to our study area (USDA Natural Resources Conservation Service, 2021). Modeled data near the upper North Fork Nooksack basin consistently

underpredicted SWE values but captured variation over time well (Figure 4). Data were downloaded as NetCDF bricks, with a time series of values stored in each grid cell of modeled monthly snowpack (SWE, in mm). The NetCDF was converted to points and trimmed to the extent of the upper North Fork Nooksack basin in ESRI ArcGIS software (ESRI, 2019). We averaged the snowpack values from each grid point over the basin area at each time step to yield one time series representing basin-scale snowpack conditions for every month from January 1950 to February 2012.

We extracted monthly Parameter-elevation Regression on Independent Slopes Model (PRISM) climatic data from 1901-2009 using ClimateWNA over a 1 kilometer grid of the North Fork Nooksack basin above USGS stream gauge no.12205000 (Hamann et al, 2013; PRISM, 2014; USGS, 2019). We averaged temperature variables and summed precipitation from each grid cell over the basin area at each time step to yield time series representing basin-scale climate conditions for every month from January 1901 to December 2009. Resulting basin-scale climatic datasets were monthly average temperature, monthly maximum temperature, monthly minimum temperature, and monthly total precipitation.

2.4 Statistical Analyses

We examined associations between basin-scale climate conditions and streamflow in the available instrumental era (1938-2009) using Pearson's correlation analysis. We correlated basin monthly average temperature, monthly maximum temperature, monthly minimum temperature, monthly total precipitation, and monthly average snowpack (SWE) with monthly average streamflow.

We examined associations between basin-scale climate conditions and tree-ring chronologies in the available instrumental era (1901-2009) using Pearson's correlations. We correlated the basin monthly climate datasets listed above with earlywood and adjusted latewood ring-width and PC chronologies.

To assess the potential for reconstruction of pre-instrumental streamflow with subannual tree-ring data, we examined associations between tree-ring chronologies and monthly average streamflow in the available instrumental era (1938-2018) using Pearson's correlation analysis. We correlated upper North Fork Nooksack monthly streamflow data with earlywood and adjusted latewood ring-width and PC chronologies.

Following assessment of reconstruction potential, we developed regression models of average August streamflow using various combinations of ring-width, PC, and backwards- and forwards-lagged chronologies as inputs. We assessed model fit using rolling forecasting origin cross-validation (80 samples, non-fixed window, minimum sample size of 36, withholding 6 values from each sample) using R package caret (Kuhn, 2008; Hyndman & Athanasopoulos, 2018). We selected the best reconstruction model based on cross-validation results and the biological plausibility of climate variable controls on tree growth. We then reconstructed average August streamflow of the upper North Fork Nooksack River from 1574-2017 using an Ordinary Least Squares (OLS) regression and identified years of exceptionally low and high streamflows.

3.0 Results

3.1 Tree-Ring Chronologies

Sixteen mountain hemlock ring-width chronologies and four principal component chronologies were developed for this study. We developed total width, earlywood width, raw latewood width, and adjusted latewood width prewhitened residual ring-width chronologies (henceforth 'ring-width chronologies') for each site location (Heather Meadows, Grouse Ridge, and Canyon Ridge), as well as regional chronologies which consisted of individual core samples from all three site locations. Table 2 provides a summary of tree core samples and crossdating statistics for total width chronologies. Figure 5 shows the site and regional total width chronologies. Total width, earlywood, raw latewood, and adjusted latewood principal component chronologies (henceforth 'PC chronologies') were calculated at the regional level, with inputs to principal components analyses being the three ring-width site chronologies for each respective annual or subannual tree-ring variable. Figure 6 shows the regional earlywood and adjusted latewood ring-width and PC chronologies. The first principal component of each tree-ring variable explained 66-86% of the variation in radial growth, indicating highly unified growth patterns in the ring-width chronologies (Table 1).

The regional ring-width chronologies contain cores from the interval 1430-2018, with at least 50 cores contributing to the latter 350 years of the chronology. Sample depth of individual series decreased progressively to 22 cores at 1600, 10 at 1550, and less than 5 from 1430-1500. To ensure that the regional chronologies captured a common signal between trees, we truncated the chronologies at 1574 based on a subsample signal strength (SSS) >0.85, with at least 12 cores contributing to each year.

Variation in total ring-width primarily reflected variation in earlywood. Unprocessed earlywood widths comprised 73% of unprocessed total ring-widths. A linear model with the regional earlywood ring-width chronology as predictor (independent variable) of the regional total ring-width chronology (dependent variable) indicated that earlywood width described 94% of the variance in total width.

Adjusted latewood chronologies were used for subsequent analyses instead of raw (non-adjusted) latewood chronologies since variation in raw latewood primarily reflected variation in earlywood, though the degree to which latewood depended on antecedent earlywood differed between sites. Earlywood described 49%, 54%, and 78% of the variance in raw latewood at Heather Meadows, Grouse Ridge, and Canyon Ridge, respectively (Figure 7). The regional adjusted latewood width chronology represents the three site adjusted latewood width chronologies averaged together.

Regional ring-width chronologies were used instead of the PC chronologies for reconstruction modeling analyses. The less-abstract ring-width chronologies produced similar but generally higher correlations with climate and streamflow variables than the PC chronologies. Most importantly, ring-width chronologies produced stronger correlations with the target reconstruction variable, average August streamflow. Furthermore, ring-width and PC chronologies were highly correlated with each other within respective seasonal pairings (Table 3). This provides further evidence of the unified signal present in the regional ring-width chronologies and their utility for dendroclimatic analysis.

3.2 Streamflow-Climate Associations

In our analysis of associations between basin-scale climate conditions and streamflow, we found significant correlations between climate variables (monthly average temperature, monthly maximum temperature, monthly minimum temperature, monthly total precipitation, monthly average snowpack (SWE)) and monthly average streamflow of the upper North Fork Nooksack River. We used Pearson's correlations with 95% and 99% confidence intervals.

Throughout the cold season, monthly average streamflow was positively correlated with average temperature of the same month (November through May). However, this changed in the warm season to a lagged pattern where summer streamflow was correlated negatively with spring average temperature (June through August streamflow correlated negatively with March through May average temperatures). This pattern continued into summer when summer streamflow was correlated negatively with summer temperatures from the preceding month (July through August streamflow correlated negatively with June through July average temperatures) (Figure 8, panel a).

Correlations between streamflow and other temperature variables (monthly maximum and minimum temperatures) closely tracked the same seasonal pattern as correlations with monthly average temperatures, with minor differences (Figure 8, panels b and c).

During the low-streamflow season (August through April), monthly average streamflow was positively correlated with total monthly precipitation of the same month. During the summer, we observed a lagged relationship between precipitation and streamflow where June-August streamflow correlated positively with January-March precipitation from earlier that year (Figure 8, panel d).

Autumn streamflow correlated positively with autumn basin snowpack (October through November). Summer streamflow correlated positively with winter, spring, and summer basin snowpack (June through August streamflow correlated with January through August basin snowpack) (Figure 8, panel e).

3.3 Climate-Growth Associations

In our examination of associations between basin-scale climate conditions and tree growth, we found significant correlations between climate variables (monthly average temperature, monthly maximum temperature, monthly minimum temperature, monthly total precipitation, monthly average snowpack) and tree-ring chronologies (regional earlywood width, earlywood PC, adjusted latewood width, adjusted latewood PC). We ran our correlation tests on the interval of the previous year's June through the same year's September. We used Pearson's correlations with 95% and 99% confidence intervals. Ring-width and PC chronologies produced highly similar correlation results, though ring-width chronologies consistently produced slightly higher correlation coefficients than PC chronologies. The following text therefore pertains to the ring-width chronologies only, though coefficients for both ring-width and PC chronologies are featured in Figure 9.

The regional earlywood width chronology showed a strong negative association with the previous year's July temperature variables (average, maximum, and minimum temperature). This pattern shifted to a positive association with temperature variables during the previous year's autumn. There were significant positive correlations with average and maximum temperatures of the same year in January, March, April, and June. Correlations with minimum temperature of the

same year were not significant, though coefficients showed a similar pattern as average and maximum temperature coefficients (Figure 9, panels a, c, & e).

The earlywood width chronology showed a positive association with the previous year's July total precipitation. This pattern shifted to a negative association with precipitation during the previous year's autumn. There were significant negative correlations with the previous year's October total precipitation and the same year's February, March, April, June, and July total precipitation. Associations between earlywood and snowpack (SWE) showed a similar pattern, although the strength of coefficients was much higher for the snowpack variable. Significant negative correlations were found for the previous year's June and July snowpack, and significant positive correlations were found for the previous year's October through the same year's August snowpack (Figure 9, panels g & i).

The regional adjusted latewood width chronology showed a strong negative association with the previous year's July, August, and October average and maximum temperatures. This pattern shifted to a positive association with average and maximum temperatures during the same year's spring. There were significant positive correlations with the same year's August average temperature and July-August maximum temperature. No significant correlations were found between adjusted latewood and minimum temperature (Figure 9, panels b, d, & f).

The adjusted latewood width chronology showed a positive association with the previous year's July, August, and November total precipitation. This pattern shifted to a negative association with total precipitation during the same year's spring. There were significant negative correlations with the same year's July and August total precipitation. Associations between adjusted latewood and snowpack followed a similar pattern, though correlation coefficients approached zero for most months with the exception of a few months with

significant correlation coefficients.There were significant positive correlations with the previous year's July and August snowpack and a significant negative correlation with the same year's August snowpack (Figure 9, panels h & j). Note that snowpack data indicates very low values, often zero, for the month of August, so the strength of correlation coefficients from this month should be interpreted with care.

3.4 Streamflow-Growth Associations

To assess the potential for reconstruction of pre-instrumental streamflow with subannual tree-ring data, we ran the same correlation testing procedure detailed above with average monthly streamflow data and tree-ring chronologies. The following text pertains to the ring-width chronologies only, though coefficients for both ring-width and PC chronologies are featured in Figure 10.

The regional earlywood width chronology showed a positive association with the previous year's average August streamflow. This pattern shifted to a negative association during the previous year's autumn. There were significant negative correlations with the same year's summer streamflows from June-August, with the highest correlation coefficient for average August streamflow at R = -0.56 (Figure 10, panel a).

The regional adjusted latewood width chronology showed a positive association with the previous year's July and August average streamflows, with the highest correlation coefficient for the previous year's average August streamflow at R = 0.26. There were no significant correlations between adjusted latewood and same-year streamflows (Figure 10, panel b).

In summary, average August streamflow signals were present in both earlywood and adjusted latewood. The earlywood signal was contained in the same calendar year (T0), while the adjusted latewood signal was contained in the year following streamflow observation (T+1).

3.5 Streamflow Reconstruction

We reconstructed average August streamflow of the upper North Fork Nooksack River from 1574-2018 using our regional earlywood ring-width chronology (T0) and forward-lagged adjusted latewood ring-width chronology (T+1). We chose this model based on cross-validation and calibration results (Table 5). Notably, models with PC chronology predictors showed marginally lower fit than models with ring-width chronology predictors.

An ordinary least squares (OLS) regression of average August streamflow with these predictors explains a moderate amount of streamflow variation (R-squared = 0.32) during the model calibration period, 1938-2017. Figure 11 shows the modeled and observed average August streamflow records over the calibration period.

Based on an acceptable replication of the observed streamflow record, we used the regional earlywood ring-width and adjusted latewood chronologies to reconstruct the average August streamflow record back to 1574 using the following equation:

$$SF_{Aug} = -890.9*EW + 362.3*LWa_{T+1} + 1328.5$$

Where:

SF_{Aug} = Average August streamflow

EW = regional earlywood chronology (ring-width indices)

LWa_{T+1} = forward-lagged regional adjusted latewood chronology (ring-width indices)

The reconstruction indicated the lowest average August streamflows (below the 1st percentile) in 1591, 1600, 1726, and 1756 (Figure 12, panel a). The most notable periods of sustained low flows were indicated from 1677-1686, 1824-1837, and 1932-1948 (Figure 13).

The reconstruction indicates the highest streamflows (above the 99th percentile) in 1587, 1715, 1810, and 1819 (Figure 12, panel b). The most notable periods of sustained high flows were indicated from 1693-1703 and 1806-1817 (Figure 13).

4.0 Discussion

4.1 Tree-Ring Chronologies

The tree-ring chronologies produced for this study were sensitive to climate and useful in dendrohydrological reconstruction models. Total ring-widths were mostly comprised of earlywood width, and earlywood width explained most of the variance in total width (94%) and raw latewood width (49-78%) prior to latewood adjustment.

Regional ring-width chronologies usually produced slightly higher correlations with climate and streamflow data than PC chronologies. This could be due to the close proximity of data collection sites and low number of ring-width site chronology inputs to Principal Components Analyses. However, the production of similar correlation coefficients between regional ring-width and PC chronologies further supports the presence of a strong, unified signal within the ring-width chronologies. We also chose the ring-width chronologies over the PC chronologies because their ring-width index values are less abstract than PC eigenvalues, making interpretation of model outputs more accessible.

Separating total ring-widths into earlywood and adjusted latewood widths increased the strength of climate signals in the tree-ring data. Correlation with June snowpack (SWE) increased from R = -0.57 for regional total width to R = -0.63 for regional earlywood width. Similarly, correlation with average August streamflow increased from R = -0.51 for total width to R = -0.56 for earlywood. Correlation with August maximum temperature went from R = -0.04 for regional total width to R = 0.32 for regional adjusted latewood width. Correlation with previous August precipitation went from R = 0.13 for total width to R = 0.39 for adjusted latewood. Correlation coefficients for all climate variables and all ring-width chronologies are available in Table 4.

Correlations between raw (non-adjusted) latewood and climate/streamflow variables demonstrated the influence of antecedent earlywood growth on raw latewood. However, adjusting latewood effectively negated this problem. For example, raw latewood was significantly correlated with June SWE at R = -0.39 but adjusted latewood was not at R = 0.002. Similarly, raw latewood was significantly correlated with average August streamflow at R = -0.37 but adjusted latewood was not at R = 0.005. Signals in the regional adjusted latewood chronology can therefore be interpreted as fundamentally different than signals in the regional earlywood chronology. The adjustment of latewood is a crucial step for anyone who wishes to use subannual ring-width measurements in dendroclimatic or dendrohydrological analyses (Meko & Baisan, 2001; Stahle et al, 2009; Griffin et al, 2011; Crawford et al, 2015).

To our knowledge, this study represents the first to use subannual ring-width measurements from mountain hemlock (*Tsuga mertensiana*) and the first to use these measurements for dendrohydrological analyses in the coastal Pacific Northwest. As such,

associations between these measurements and climate/streamflow variables are not well understood and our findings represent an initial investigation.

We chose to adjust latewood at the site chronology level after Meko & Baisan (2001) and Stahle et al (2009), despite the recommendation from Griffin et al (2011) to make the adjustment at the core level. We were most interested in how earlywood and adjusted latewood associate with climate in this environment, and Griffin et al (2011) indicated no difference in climate-growth associations whether latewood was adjusted at the site or core level. We did however find large differences between sites in the degree to which raw latewood depended on antecedent earlywood. 49%, 54%, and 78% of the variance in raw latewood was explained by antecedent earlywood at Heather Meadows, Grouse Ridge, and Canyon Ridge, respectively. It is reasonable to suspect that there was also a range of variance in dependence within sites (between individual trees). As with any tree-growth metric, the dependence of raw latewood on antecedent earlywood could be affected by a number of factors between and within sites such as aspect, light intensity, geology, soils, local hydrology, understory vegetation, and mycorrhizal network (Kozlowski & Pallardy, 1997; Cazares et al, 2005).

Although we found the calculation of adjusted latewood at the site level to be adequate for the purpose of reconstructing streamflow, future studies could reveal more nuanced relationships by exploring the option to calculate adjusted latewood at the level of individual cores. Adjusting latewood at the core level would allow for within-tree analyses like testing whether variance in latewood width diminishes over time in exceptionally old trees, as was visually observed in Douglas-fir and Ponderosa Pine in New Mexico by Stahle et al (2009) and to a lesser extent in Douglas-fir in Arizona by Griffin et al (2011). Griffin et al (2011) advocated for including young and middle-aged trees to counteract this effect so that any problematic

latewood measurements from elderly samples can be sorted out during the crossdating process by the weighted mean. The maximum lifespan of mountain hemlock trees is estimated at approximately 700 years (Peterson & Peterson, 2001). While some of our samples approached 600 years of age, in total our samples had an average series length of 324 years, and 30 of 113 samples had a series length less than 250 years. Our data therefore likely contains sufficient measurements from young and middle-aged trees, with the caveat that we are working with a different species in a different environment than Stahle et al (2009) and Griffin et al (2011).

4.2 Climate Controls on Streamflow

The timing of peak and low flows in instrumental streamflow data and the results of correlation tests with climate data support the classification of the upper North Fork Nooksack basin as a mixed rain-and-snow dominant system, with the heaviest influence coming from snowmelt.

Instrumental data show a small, rain-driven runoff peak in November. This peak diminishes throughout the snow accumulation season until the melt season begins in March, with a large, snowmelt-driven runoff peak centered in June and decreasing summer flows until the autumn rain season (Figure 2, Figure 3).

Correlation results show that winter through summer snowpack drives summer streamflows. Greater snowpack accumulation and persistence into the summer season supports higher summer streamflows. Correlation coefficients were strongest between streamflow and snowpack from the preceding month (Figure 8, panel e). August streamflow was correlated with July snowpack at R = 0.73. July streamflow was even more sensitive to snowpack, with a correlation of R= 0.79 with June snowpack.

Significant correlations between streamflow and late summer, autumn, and winter precipitation of the same month could indicate the influence of rain events on streamflow. The highest correlation coefficients occur in late autumn and early winter (up to R = 0.69), when rainfalls are heavy and rain-on-snow events produce high streamflow events (Figure 8, panel d).

Correlation results between streamflow and temperature variables likely indicate temperature controls on snowmelt and whether precipitation falls as rain or snow. Warmer temperatures during the spring and early summer melt season were associated with lower streamflows in the following months (up to R = -0.51), likely due to early reduction in snowpack and early end of the snowmelt season. There were significant positive correlations between streamflow and temperatures of the same month from late autumn through May (up to R = 0.67), when above-freezing temperatures can switch would-be snowfall to rain. When combined with an existing snowpack, this could create rain-on-snow high flow events.

Both instrumental and modeled average August streamflow inter-annual variability matched expectations for a mixed rain-and-snow basin. In such a basin, August streamflow should vary highly from year to year and not relate to streamflow from preceding years (Coulthard & Smith, 2016). No serial autocorrelation was found in instrumental or modeled streamflow.

4.3 Climate Controls on Radial Growth

Results of our climate-growth correlation analyses are consistent with previous studies on mountain hemlock in the Pacific Northwest (Brubaker, 1980; Graumlich & Brubaker, 1986; Woodward et al, 1994; Smith & Laroque, 1998; Gedalof & Smith, 2001; Peterson & Peterson, 2001; Ettinger et al, 2011; Pitman & Smith, 2013; Marcinkowski et al, 2015).

Persistence and melt timing of the snowpack determines the start of the growing season, leaving a snowpack signal in mountain hemlock ring-widths (Smith & Laroque, 1998). Like many other conifer species growing at the upper elevation treeline, mountain hemlocks do not begin water uptake or increase respiration until soils reach above-freezing temperatures (Graumlich & Brubaker, 1986; Peterson & Peterson, 1994; Gedalof & Smith, 2001; Peterson & Peterson, 2001). Mountain hemlock roots are typically shallow in subalpine environments due to low nutrient availability in poorly-developed soils, leaving them particularly susceptible to freeze/thaw soil moisture dynamics (Kozlowski & Pallardy, 1997). Positive correlations between earlywood and same-year spring and early summer temperatures (up to R = 0.26 in April) and early summer snowpack (up to R = -0.63 in June) support all of these findings in our samples.

Further evidence of a snowpack limitation on tree growth can be seen in particularly high and low snowpack years from recent memory, water years 1999 and 2015, respectively. In 1999, Mount Baker Ski Area (directly adjacent to the Heather Meadows study site) recorded a world record winter snowfall of 1,140 in (2,896 cm) (Leffler et al, 2001). Our cross-dating results show that a characteristically narrow growth ring formed throughout our tree-ring samples in the following growth season. Conversely, in 2015 the same location recorded a snowfall total of only 303 in (770 cm). Our cross-dating results show a characteristically wide growth ring formed throughout our tree-ring samples in the following growth season.

Summer temperature and precipitation of the same and previous year also leave growth signals in mountain hemlock ring-widths (Graumlich & Brubaker; Gedalof & Smith, 2001; Peterson & Peterson, 2001). High early summer temperatures and low early summer precipitation were associated with greater earlywood widths (up to R = 0.25 for June average temperature, and R = -0.22 for June precipitation). High late summer temperatures and low late

summer precipitation in the same year were associated with greater adjusted latewood widths (up to R = 0.32 for August maximum temperature, and R = -0.19 for August precipitation) (Figure 9). Peterson & Peterson (1994) speculate that this association in annual ring-width could be a result of light intensity and photosynthetic potential for subalpine larch (*Larix lyallii*), subalpine fir (*Abies lasiocarpa*), and Engelmenn spruce (*Picea engelmannii*) in the North Cascades. This could also be true for mountain hemlocks growing in the same subalpine environment, where a cloudy growing season might limit growth via low light, cool temperatures, and low levels of photosynthesis.

Temperature and precipitation signals from the previous year's summer, however, were opposite and stronger than the same-year signals. High early summer temperature and low early summer precipitation in the previous year were associated with lower earlywood widths (up to R = -0.46 for previous July maximum temperature, and R = 0.23 for previous July precipitation). High temperature and low precipitation in the previous year were associated with lower adjusted latewood widths (up to R = -0.32 for previous August maximum temperature, and R = 0.39 for previous August precipitation) (Figure 9). Life cycle processes have been cited by others to explain this association (Woodward et al, 1994; Gedalof & Smith, 2001; Peterson & Peterson, 2001). In a 30-year study on cone production, Woodward et al (1994) observed that optimal conditions for cone production in mountain hemlock were the opposite of optimal conditions for radial growth. Specifically, high temperatures in the previous year's summer were associated with a large cone crop and low radial growth. Our samples also followed this pattern. Woodward et al (1994) concluded that sample trees had finite energy stores and could allocate more energy towards cone production or radial growth as needed.

Until this study, these climate signals had only been documented in mountain hemlock annual rings (total ring-width), but we found that signal strengths typically increased when total widths were separated into earlywood and adjusted latewood. Using subannual proxies provides a more nuanced view of climate-growth associations by partitioning the climate signal recorded in ring widths into different portions of the growing season. Earlywood was strongly correlated with winter through summer snowpack, and showed an improved snowpack correlation compared to total width of up to 6%. Adjusted latewood showed more drastic changes in signal quality and strength compared to total width, due to its relatively small portion of total width and dependence on antecedent earlywood width. Of particular note were improvements in correlations with late summer temperature and precipitation when compared to total width. Correlation with same-year maximum August temperature increased by 28%, same-year August precipitation increased by 13%, previous-year August maximum temperature increased by 19%, and previous-year August precipitation increased by 13% (Table 3). The portion of latewood that was not determined by antecedent earlywood growth was likely subject to climate conditions happening in and around the month of August, after which the growing season presumably ends. Correlations with climate variables near R = 0 in September also support this observation.

4.4 Streamflow Reconstruction with Subannual Predictors

Streamflow of the upper North Fork Nooksack River is largely driven by snowpack quantity and melt timing (Bach, 2002; Dickerson-Lange & Mitchell, 2014; Murphy, 2016). High-elevation mountain hemlock radial growth is also largely driven by snowpack quantity and melt timing, as the tree growing season starts and ends when snow no longer covers roots and soil temperatures are above freezing (Brubaker, 1980; Heikkinen, 1985; Graumlich & Brubaker,

1986; Woodward et al, 1994; Smith & Larocque, 1998; Gedalof & Smith, 2001; Peterson & Peterson, 2001).

Separating total ring-widths into earlywood and adjusted latewood widths strengthened the streamflow signal available in our tree-ring data. Correlation analyses between subannual tree-ring variables and climate variables showed that streamflow and earlywood widths were indirectly connected via snowpack and same-year warm season temperature and precipitation, while previous-year streamflow and same-year adjusted latewood widths were indirectly connected via previous-year snowpack, previous-year warm season temperature, and previous-year warm season precipitation. Separating earlywood and adjusted latewood also allowed us to lag the adjusted latewood chronology forward by one year to take advantage of its previous-year streamflow signal in addition to the strong earlywood same-year streamflow signal.

A reconstruction model (Ordinary Least Squares regression) based on total ring-width alone explained 25% of the variance in average August streamflow. A model based on earlywood alone explained 30% variance, and a model with earlywood (T=0) and forward-lagged adjusted latewood (T+1) explained 32% variance. While these models did not explain a high amount of streamflow variance compared to studies that used more complex techniques such as such as integrated tree-ring and hydrological modeling (Lutz et al, 2012), combining tree-ring and independently-reconstructed PDSI or PDO predictors (Coulthard et al, 2016; Mood & Smith, 2021), and measurement of tree-ring maximum density (Starheim et al, 2013), we would like to note that we explained an additional 7% of the variance in streamflow by using subannual predictors rather than annual ring-widths. If subannual measurements were used in tandem with more complex techniques, streamflow reconstructions in the coastal Pacific Northwest could be improved.

We postulate that mountain hemlock subannual ring-width measurements could also be useful in snowpack reconstructions. This study did not reconstruct snowpack due to the lack of long-term instrumental data near the study area. However, with modeled snowpack data from Hostetler & Alder (2016) we observed up to a 6% increase in correlation between snowpack and earlywood compared to total ring-width.

4.5 Streamflow Reconstruction Model in Hydrological Context

Our streamflow reconstruction underpredicted observed higher-magnitude average August streamflows, but did passably well at predicting the magnitude of low flows and capturing trends in above- and below-average flows (Figure 11). This is a common problem with tree-ring reconstructions of streamflow, which assume a linear relationship between tree growth and streamflow (Gedalof et al, 2004; Hart et al, 2010; Starheim et al, 2013; Coulthard & Smith, 2016; Littell et al, 2016). A residual plot of our reconstruction model indicates possible minor non-linearity, but well below statistical significance.

High-elevation mountain hemlock radial growth and upper North Fork Nooksack basin August streamflow responded to a similar suite of climate conditions. Radial tree growth and streamflow are fundamentally different variables though, leaving a large amount of streamflow variance not explained by tree growth. Not only do trees respond differently to the same climate conditions as streamflow, their radial growth is subject to a host of factors that do not affect streamflow, such as cone production (Woodward et al, 1994). Conversely, streamflow is subject to a number of conditions throughout the watershed that trees at our high-elevation subalpine parkland sites were not subject to, such as glacier melt runoff and land use changes at lower elevations (Matheussen et al, 2000; Bach, 2002; Dickerson-Lange & Mitchell, 2014; Pelto, 2015;

Murphy, 2016). We discuss these differences and their implications for our streamflow reconstruction at greater length in the following paragraphs.

Tree life-cycle processes, potential non-stationarity in climate-growth response, and differences between study site characteristics could increase noise in radial growth signals and lower the predictive power of our reconstruction model. As discussed in the 'Climate Controls on Radial Growth' section above, life cycle processes such as cone production can divert tree internal energy resources away from radial growth (Woodward et al, 1994). The same tree could therefore put on a different amount of radial growth under the same climate conditions depending on whether it was in the first or second year of its reproductive cycle. Fortunately, reproductive processes are also highly responsive to climate conditions, partially reducing this effect (Woodward et al, 1994). Another factor which could introduce noise in radial growth signals and lower the predictive power of our reconstruction model was an observation by Marcinkowski et al (2015) of possible non-stationary climate responses in mountain hemlock annual rings throughout the North Cascades. They found a reduction in snowpack correlation to the point of non-significance after the year 2000. We tested for this potential problem in our data and found it not true for radial growth correlations with snowpack or average August streamflow. Lastly, trees are complex biological beings and are subject to a host of large- and small-scale factors beyond climate and reproductive processes. They are affected by aspect, light intensity, geology, soils, local hydrology, understory vegetation, mycorrhizal network, herbivory, and other factors that vary between and within study sites (Kozlowski & Pallardy, 1997; Cazares et al, 2005).

Glacier melt in late summer could contribute to higher average August streamflows than were detected by our tree-ring data. Summer glacial melt runoff is well documented in the North

Fork Nooksack basin (Bach, 2002; Dickerson-Lange & Mitchell, 2014; Pelto, 2015; Murphy, 2016). The snow that built the glaciers fell potentially centuries before glacial meltwater reached the stream channel. Tree growth rings would document this snowfall at the time it occurred rather than the time it melted and flowed down the stream channel. Murphy (2016) places the timing of maximum annual glacier melt inputs to the months of August and September. This could explain some of our reconstruction model's underprediction of August streamflow. This effect could be partially accounted for by the late summer temperature signals in our tree-ring data, which also govern the rate of glacial melt. Trends in reconstructed August streamflows mostly coincide with Coleman Glacier moraine dates found by Heikkinen (1984). The Coleman Glacier drains into the upper North Fork Nooksack basin, and periods of sustained increasing streamflow in our reconstructed record follow moraine dates given by Heikkinen (1984) in 1740, 1823, 1855-1856, 1886-1887, and 1908-1912 (Figure 13). The only moraine dates not followed by an increase in reconstructed August flows are those dated to 1922 and 1978-1979. An increase in August flow following the 1978-1979 moraine is visible in observed streamflow data, however. Streamflow of snow-dominant but non-glaciated streams might be better candidates for reconstruction (Starheim et al, 2013; Coulthard & Smith, 2016; Mood et al, 2021) than glaciated streams due to noise from glacial meltwater inputs not documented by tree-rings during the same year.

Land use changes such as timber harvest have been shown to increase the variability of summer streamflow in the Columbia River basin (Matheussen et al, 2000). Forest once covered the entirety of the North Fork Nooksack basin prior to European settlement but lower portions of the upper basin have been logged since the 1930s (Bach, 2002). In the Columbia Basin, Matheussen et al (2000) observed greater snow accumulation and greater spring runoff in logged

areas, which led to more variability in summer streamflows. The effects of timber harvest activity were somewhat offset by fire suppression in the Columbia basin, but this was not likely at play in the North Fork Nooksack basin since fire return intervals on the west slopes of the North Cascades are naturally multiple centuries (Halofsky et al, 2018). Regardless, the hydrological effects of timber harvest or fire suppression at lower elevations would not be detected by our high-elevation, subalpine sample trees. Variations in streamflow due to land use changes therefore represent another source of potential noise and could lower the predictive power of our reconstruction model.

Reconstructed average August streamflows prior to climate change and European settlement may be more accurate than later reconstructed flows due to the potential noise from increased glacial melt and timber harvest discussed above. The instrumental streamflow record begins in 1938, decades after the start of anthropogenic climate change and shortly after the start of logging activity in the upper basin. Matches between increased reconstructed flow values and Coleman glacier moraine dates from Heikkinen (1984) indicate some strength in our streamflow reconstruction prior to instrumental data.

4.6 Streamflow Reconstruction Implications for Water Resources

Studying historical periods of streamflow drought and surplus could help us prepare for future water resource planning. City governments have even provided funding to tree-ring researchers to reconstruct pre-instrumental streamflows in municipal watersheds (Mood & Smith, 2021). While our particular streamflow reconstruction model did not capture the magnitude of high average August streamflows during the model calibration period, it did passably well at capturing the magnitude of low flows and trends in sustained above- and below-

average flows. However, interpretation of this reconstructed record should be approached with caution.

Our reconstruction indicates that the most extreme low flows (below the 1st percentile) may have all occurred in or before 1756 (Figure 12, panel a). The most extreme high flows (above the 99th percentile) may have all occurred in or before 1819 (Figure 12, panel b), although the accuracy of predicted high flows should be interpreted critically. Greater extremes in the earlier portion of the reconstructed record could be due to greater inter-annual fluctuations in snowpack. Temperature in the Pacific Northwest began warming around 1830, at the end of the Little Ice Age period (Heikkinen, 1984), which could correspond to lower snowpack accumulation and variability in late summer streamflow after this date. Higher extremes in the reconstructed record could also be an artifact of lower tree-ring sample depths contributing to the early portions of tree-ring chronologies. However, we trimmed chronologies to an appropriate Subsample Signal Strength (SSS > 0.85) at the year 1574, with at least 50 cores contributing to ring-width chronologies after 1662.

Both observed and modeled streamflow showed high inter-annual variability, making identification of multi-year droughts or surpluses difficult at a glance. But a simple 9-year rolling mean of annual reconstructed flow volumes highlighted periods of generally above- or below-average flows (Figure 13). The reconstruction indicated longer multi-year droughts and surpluses than were present in the instrumental data, on the order of 10-15 years rather than 5-7 years. Water resource managers might therefore consider preparing for these longer naturally-occuring droughts, let alone droughts that might occur under future climate conditions (Coulthard et al, 2016).

The most common concern cited by researchers and water resource managers for the Nooksack basin is the loss of glaciers in a warming climate (Bach, 2002; Grah & Beaulieu, 2013; Dickerson-Lange & Mitchell, 2014; Pelto, 2015; Murphy, 2016). As glaciers shrink they contribute decreasing volumes of meltwater to late summer streamflow (Stahl et al, 2006; Stahl & Moore, 2006; Moore et al, 2009; Murphy, 2016). Striking glacier retreats have been observed on Mount Baker, where Pelto & Brown (2012) estimated a 12-20% loss in glacier volume from 1990-2010 alone. Murphy (2016) modeled glacier inputs to streamflow in the North Fork Nooksack basin under potential future climate conditions, and found that glacial meltwater inputs to late summer streamflow could drop from 51% in 30-year normal streamflow in 2025 to approximately 25% in 2075. Glacier melt currently acts as a buffer for low late summer streamflows, increasing meltwater supply during warm, dry years. Their diminishment and eventual disappearance will greatly affect late summer streamflow volumes.

5.0 Conclusion

We reconstructed average August streamflow of the upper North Fork Nooksack basin in the Cascade Mountains of northern Washington State, U.S.A. to the year 1574 using subannual ring-width measurements from mountain hemlock trees. Late summer streamflows in transient rain-and-snow watersheds are expected to change drastically in response to future climate change, which makes understanding historical flows increasingly important. We explained an additional 7% of the variance in August streamflow by separating total ring-widths into earlywood and adjusted latewood widths.

Our methods required less skill, time, and money than other, more complex methods being employed locally such as integrated tree-ring and hydrological modeling (Lutz et al, 2012), combining tree-ring and independently-reconstructed PDSI or PDO predictors (Coulthard et al, 2016; Mood & Smith, 2021), and measurement of tree-ring maximum density (Starheim et al, 2013). Our reconstruction model did not explain a high amount of variance in August streamflow, however model improvements with subannual ring-widths over annual ring-widths leads us to advocate for the expansion of earlywood and latewood chronologies in the Pacific Northwest. Especially when used in tandem with more complex techniques, subannual measurements could significantly improve the skill of hydroclimate reconstruction models.

6.0 References

Abram, N.J., McGregor, H.V., Tierney, J.E., Evans, M.N., McKay, N.P., Kaufman, D.S., The PAGES 2k Consortium (2016). Early onset of industrial-era warming across the oceans and continents. *Nature, 536,* 411-418.

Alder, J. R., & Hostetler, S. W. (2018). The Dependence of Hydroclimate Projections in Snow-Dominated Regions of the Western United States on the Choice of Statistically Downscaled Climate Data. *Water Resources Research, 55(3),* 2279-2300.

Bach, A. (2002). Contributions to the Nooksack River Watershed, North Cascades Range, Washington. *Geographical Review, 92(2),* 192-212.

Barnett, T.P., Adam, J.C., Lettenmaier, D.P. (2005). Potential impacts of a warming climate on water availability in snow-dominated regions. *Nature Reviews, 438,* 303-309.

Brewer, P.W. (2014). Data Management in Dendroarchaeology Using Tellervo. *Tree-Ring Research, 70(3),* S79-S83.

Brubaker, L.B. (1980). Spatial Patterns of Tree Growth Anomalies in the Pacific Northwest. *Ecology, 61(4),* 798-807.

Bunn, A.G. (2008). A Dendrochronology Program Library in R (dplR). *Dendrochronologia, 26(2),* 115-124.

Bunn, A.G. (2012). Heather Meadows – Mt Baker – TSME – ITRDB WA134.

Buras, A. (2017). A comment on the Expressed Population Signal. *Dendrochronologia, 44,* 130-132.

Cazares, E., Trappe, J.M., Jumponnen, A. (2005). Mycorrhiza-plant colonization patterns on a subalpine glacier forefront as a model system of primary succession. *Mycorrhiza, 15,* 405-416.

Cook, E.R., & Kairiukstis, L.A. (Eds.). (1990). *Methods of Dendrochronology: Applications in the Environmental Sciences*. Kluwer Academic Publishers.

Coulthard, B.L., Anchukaitis, K.J., Pederson, G.T., Cook, E., Littell, J., Smith, D.J. (2021). "Snowpack Signals in North American Tree Rings." *Environmental Research Letters, 16(3),* 034037.

Coulthard, B., & Smith, D.J. (2016). A 477-year dendrohydrological assessment of drought severity for Tsable River, Vancouver Island, British Columbia, Canada. *Hydrological Processes, 30,* 1676-1690.

Coulthard, B., Smith, D.J., Meko, D.M. (2016). Is worst-case scenario streamflow drought underestimated in British Columbia? A multi-century perspective for the south coast, derived from tree-rings. *Journal of Hydrology, 534,* 205-218.

Crawford, J.C., Griffin, D., Kipfmueller, K.F. (2015). Capturing season-specific precipitation signals in the northern Rocky Mountains, USA, using earlywood and latewood tree rings. *Journal of Geophysical Research: Biogeosciences, 120,* 428-440.

Dickerson-Lange, S.E., & Mitchell, R. (2014). Modeling the effects of climate change projections on streamflow in the Nooksack River Basin, Northwest Washington. *Hydrological Processes, 28,* 5236-5250.

Dierauer, J.R., Allen, D.M., Whitfield, P.H. (2019). Snow Drought Risk and Susceptibility in the Western United States and Southwestern Canada. *Water Resources Research 55(4),* 3076–3091.

Dudley, R.W., Hodgkins, H.A., McHale, M.R., Kolian, M.J., Renard, B. (2017). Trends in Snowmelt-Related Streamflow Timing in the Conterminous United States. *Journal of Hydrology, 547,* 208-221.

ESRI (2019). ArcGIS Pro: Version 2.1. Redlands, CA: Environmental Systems Research Institute.

Ettinger, A.K., Ford, K.R., HilleRisLambers J. (2011). Climate determines the upper, but not lower, altitudinal range limits of Pacific Northwest conifers. *Ecology, 92(6),* 1323-1331.

Fountain, A.G., & Tangborn, W.V. (1985). The Effect of Glaciers on Streamflow Variations. *Water Resources Research, 21(4),* 579-586.

Fritts, H.C. (1976). *Tree rings and climate*. Academic Press, London, United Kingdom.

Fritts, H.C., J. Guiot, G.A. Gordon, and F. Schweingruber, 1990. Methods of Calibration, Verification, and Reconstruction. *In: Methods of Dendrochronology: Applications in the Environmental Sciences,* E.R. Cook and L.A. Kairiukstis (Editors). Kluwer Academic Publishers, Dordrecht, Netherlands, 163-217.

Gedalof, Z., Peterson, D.L., Mantua, N.J. (2004). Columbia River flow and drought since 1750. *Journal of the American Water Resources Association, 40(6),* 1579-1592.

Gedalof, Z., & Smith, D.J. (2001). Dendroclimatic response of mountain hemlock (*Tsuga mertensiana*) in Pacific North America. *Canadian Journal of Forest Research, 31,* 322-332.

Grah, O., & Beaulieu, J. (2013). The effect of climate change on glacier ablation and baseflow support in the Nooksack River basin and implications on Pacific salmonid species protection and recovery. In *Climate Change and Indigenous Peoples in the United States* (149-162). Springer.

Granshaw, F.D., & Fountain, A.G. (2006). Glacier Change (1958-1998) in the North Cascades National Park Complex, Washington, USA. *Journal of Glaciology, 52(177),* 251-256.

Graumlich, L.J., & Brubaker, L.B. (1986). Reconstruction of annual temperature (1590-1979) for Longmire, Washington, derived from tree rings. *Quaternary Research, 25,* 223-234.

Griffin, D., Meko, D.M., Touchan, R., Leavitt, S.W., Woodhouse, C.A. (2011). Latewood chronology development for summer-moisture reconstruction in the US Southwest. *Tree-Ring Research, 67(2),* 87-101.

Halofsky, J.S., Conklin, D.R., Donato, D.C., Halofsky, J.E., Kim, J.B. (2018). Climate change, wildfire, and vegetation shifts in a high-inertia forest landscape: Western Washington, U.S.A. *PLoS ONE 13(12),* e0209490.

Hamann, A., Wang, T., Spittlehouse, D.L., Murdock, T.Q. (2013). A comprehensive high-resolution database of historical and projected climate surfaces for western North America. *Bulletin of the American Meteorological Society, 94,* 1307-1309.

Hamlet, A.F., Mote, P.W., Clark, M.P., Lettenmaier, D.P. (2005). Effects of Temperature and Precipitation Variability on Snowpack Trends in the Western United States. *Journal of Climate, 18,* 4545-4561.

Hamlet, A.F., Mote, P.W., Clark, M.P., Lettenmaier, D.P. (2007). Twentieth-Century Trends in Runoff, Evapotranspiration, and Soil Moisture in the Western United States. *Journal of Climate, 20,* 1468-1486.

Harley, G.L., Maxwell, R.S., Black, B.A., Bekker, M.F. (2020). A multi-century, tree-ring-derived perspective of the North Cascades (USA) 2014-2016 snow drought. *Climatic Change, 162,* 127-143.

Hart, S.J., Smith, D.J., Clague, J.J. (2010). A multi-species dendroclimatic reconstruction of Chilko River streamflow, British Columbia, Canada. *Hydrological Processes, 24,* 2752-2761.

Heikkinen, O. (1984). Dendrochronological evidence of variations in Coleman Glacier, Mount Baker, Washington, U.S.A. *Arctic and Alpine Research, 16(1),* 53-64.

Heikkinen, O. (1985). Relationships between tree growth and climate in the subalpine Cascade Range of Washington, U.S.A. *Annales Botanici Fennici*, 1-14.

Holmes, R.L. (1983). Computer-assisted quality control in tree-ring dating and measurement. *Tree-Ring Bulletin, 43,* 69-78.

Hostetler, S.W., & Alder, J.R. (2016). Implementation and evaluation of a monthly water balance model over the US on an 800m grid. *Water Resources Research, 52(12),* 9600-9620.

Hyndman, R.J., & Athanasopoulos, G. (2018). *Forecasting: principles and practice,* 2nd edition. OTexts, Melbourne, Australia.

Isaak, D. J.; Wollrab, S.; Horan, D.; Chandler, G. (2011). Climate change effects on stream and river temperatures across the northwest U.S. from 1980-2009 and implications for salmonid fishes. *Climatic Change, 113,* 499-524.

Kozlowski, T.T., & Pallardy, S.G. (1997). *Physiology of Woody Plants.* Academic Press, San Diego, California.

Kuhn, M. (2008). caret: Classification and Regression Training. *Journal of Statistical Software, 28(5).*

Leffler, R. J., Changery, M., Redmond, K. T., Downs, R., Taylor, G., Horvitz, A. (2001). Evaluation of a national seasonal snowfall record at the Mount Baker, Washington, Ski Area. *National Weather Digest, 25(1/2),* 15-20.

Leung, L.R., & Wigmosta, M.S. (1999). Potential climate change impacts on mountain watersheds in the Pacific Northwest. *Journal of the American Water Resources Association, 35(6),* 1463-1471.

Li, D., Wrzesien, M.L., Durand, A.J. & Lettenmaier, D. P. (2017). How much runoff originates as snow in the western United States, and how will that change in the future? *Geophysical Research Letters, 44,* 6163-6172.

Littell, J.S., Pederson, G.T., Gray, S.T., Tjoelker, M., Hamlet, A.F., Woodhouse, C.A. (2016). Reconstructions of Columbia River Streamflow from Tree-Ring Chronologies in the Pacific Northwest, USA. *Journal of the American Water Resources Association, 52(5),* 1121-1141.

Luce, C.H., & Holden, Z.A. (2009). Declining annual streamflow distributions in the Pacific Northwest United States, 1948-2006. *Geophysical Research Letters, 36,* L16401.

Lutz, E.R., Hamlet, A.F., Littell, J.S. (2012). Paleoreconstruction of cool season precipitation and warm season streamflow in the Pacific Northwest with applications to climate change assessments. *Water Resources Research, 48,* W01525.

Mantua, N., Tohver, I.M., Hamlet, A.F. (2010). Climate change impacts on streamflow extremes and summertime stream temperature and their possible consequences for freshwater salmon habitat in Washington State. *Climatic Change, 102,* 187-223.

Marcinkowski, K., Peterson, D.L., Ettl, G.J. (2015). Nonstationary Temporal Response of Mountain Hemlock Growth to Climatic Variability in the North Cascade Range, Washington, USA. *Canadian Journal of Forest Research, 45(6),* 676-688.

Matheussen, B., Kirschbaum, R.L., Goodman, I.A., O'Donnell, G.M., Lettenmaier, D.P. (2000). Effects of Land Cover Change On Streamflow in the Interior Columbia River Basin (USA and Canada). *Hydrological Processes 14,* 867-885.

Meko, D. M., & Baisan, C.H. (2001). Pilot study of latewood-width of conifers as an indicator of variability of summer rainfall in the North American Monsoon region. *International Journal of Climatology, 21,* 697-708.

Meko, D.M., Therrell, M.D., Baisan, C.H., Hughes, M.K. (2001). Sacramento River Flow Reconstructed to A.D. 869 From Tree Rings. *Journal of the American Water Resources Association, 37(4),* 1029-1039.

Mood, B.J., Coulthard, B., Smith, D.J. (2020). Three hundred years of snowpack variability in southwestern British Columbia reconstructed from tree-rings. *Hydrological Processes, 34(25),* 5123-5133.

Mood, B.J., & Smith, D.J. (2021). A multi-century July-August streamflow reconstruction of Metro Vancouver's water supply contribution from the Capilano and Seymour watersheds in southwestern British Columbia, Canada. *Canadian Water Resources Journal, 46(3),* 121-138.

Moore, R.D., Fleming, S.W., Menounos, B., Wheate, R., Fountain, A., Stahl, K., Holm, K., Jakob, M. (2009). Glacier Change in Western North America: Influences on Hydrology, Geomorphic Hazards and Water Quality. *Hydrological Processes, 23,(1),* 42-61.

Mote, P. W., Li, S., Lettenmaier, D.P., Xiao, M., Engel, R. (2018). Dramatic Declines in Snowpack in the Western US. *npj Climate and Atmospheric Science, 1*.

Mote, P.W., Hamlet, A.F., Clark, M.P., Lettenmaier, D.P. (2005). Declining Mountain Snowpack in Western North America. *American Meteorological Society*, 39-49.

Mote, P.W., Petersen, A., Reeder, S., Shipman, H., Whitely-Binder, L. (2008). *Sea level rise in the coastal waters of Washington State.* A report by the University of Washington Climate Impacts Group and the Washington Department of Oceanography.

Murphy, R.D., (2016). *Modeling the Effects of Forecasted Climate Change and Glacier Recession on late Summer Streamflow in the Upper Nooksack River Basin* (Master's thesis). Available from Western Washington University CEDAR.

Payne, J.T., Wood, A.W., Hamlet, A.F., Palmer, R.N., Lettenmaier, D.P. (2004). Mitigating the Effects of Climate Change on the Water Resources of the Columbia River Basin. *Climatic Change, 62,* 233-256.

Peel, M.C., Finlayson, B.L., McMahon, T.A. (2007). Updated world map of the Koppen-Geiger climate classification. *Hydrology and Earth System Sciences, 11,* 1633-1644.

Pelto, M.S. (2015). *Climate Driven Retreat of Mount Baker Glaciers and Changing Water Resources.* Springer International Publishing, Switzerland.

Pelto M.S., & Brown, C. (2012). Mass balance loss of Mount Baker, Washington glaciers 1990–2010. *Hydrological Processes 26(17),* 2601-2607.

Peters, K., Jacoby, G.C., Cook, E.R. (1981). Principal components analysis of tree-ring sites. *Tree-Ring Bulletin, 41,* 1-19.

Peterson, D.W., & Peterson, D.L. (1994). Effects of climate on radial growth of subalpine conifers in the North Cascade Mountains. *Canadian Journal of Forest Research, 24,* 1921-1932.

Peterson, D.W., & Peterson, D.L. (2001). Mountain hemlock growth responds to climatic variability at annual and decadal time scales. *Ecology, 82(12),* 3330-3345.

Peterson, D.W., Peterson, D.L., Ettl, G.J. (2002). Growth responses of subalpine fir to climatic variability in the Pacific Northwest. *Canadian Journal of Forest Research, 32,* 1503-1517.

Pitman, K.J., & Smith, D.J. (2013). A dendroclimatic analysis of mountain hemlock (*Tsuga mertensiana*) ring-width and maximum density parameters, southern British Columbia Coast Mountains, Canada. *Dendrochronologia, 31,* 165-174.

PRISM Climate Group (2014). Data available on the World Wide Web at https://prism.oregonstate.edu, accessed [January, 2019]. Oregon State University, Corvallis, Oregon.

R Core Team (2022). *R: A language and environment for statistical computing*. R Foundation for Statistical Computing, Vienna, Austria.

Smith, D.J., & Laroque, C.P. (1998). Mountain Hemlock Growth Dynamics on Vancouver Island. *Northwest Science, 72(2),* 67-70.

Speer, J.H. (2010). *Fundamentals of Tree Ring Research*. University of Arizona Press, Tucson, Arizona.

Stahl, K., & Moore, R.D. (2006). Influence of watershed glacier coverage on summer streamflow in British Columbia, Canada. *Water Resources Research, 42,* W06201.

Stahl, K., Moore, R.D., Shea, J.M., Hutchinson, D., Cannon, A.J. (2006). Coupled modelling of glacier and streamflow response to future climate scenarios. *Water Resources Research, 44*, W02422.

Stahle, D., Cleveland, M.K, Griffin, R.D., Fye, F.K., Therrell, M.D., Burnette, D.J., Meko, D.M., Diaz, J.V. (2009). Cool- and Warm-Season Precipitation Reconstructions over western New Mexico. *Journal of Climate, 22(13),* 3729-3750.

Starheim, C.C.A., Smith, D.J., Prowse, T.D. (2013). Dendrohydroclimate reconstructions of July-August runoff for two nival-regime rivers in west central British Columbia. *Hydrological Processes, 27,* 405-420.

Stewart, I.T., Cayan, D.R., Dettinger, M.D. (2005). Changes toward Earlier Streamflow Timing across Western North America. *Journal of Climate, 18,* 1136-1155.

Stokes, M.A., & Smiley, T.L., (1964). *An Introduction to Tree-Ring Dating.* University of Chicago Press, Chicago, Illinois, USA.

Tohver, I.M., Hamlet, A.F., Lee, S.Y. (2014). Impacts of 21-st century climate change on hydrologic extremes in the Pacific Northwest region of North America. *Journal of the American Water Resources Association, 50(6),* 1461-1476.

Trinies, C.A. (2019). *Dendroclimatology of yellow cedar (Callitropsis nootkatensis) and late Holocene temperature variability on the western slopes of the North Cascades in Washington State* (Master's thesis). Available from Western Washington University CEDAR.

Truitt, S.E. (2018). *Modeling the Effects of Climate Change on Stream Temperature in the Nooksack River Basin* (Master's thesis). Available from Western Washington University CEDAR.

USDA Natural Resources Conservation Service (2021). SNOwpack TELemetry Network (SNOTEL). NRCS.Data available on the World Wide Web at https://data.nal.usda.gov/dataset/snowpack-telemetry-network-snotel, accessed [January, 2022].

U.S. Geological Survey (2019). *National Water Information System.* Data available on the World Wide Web (Water Data for the Nation), accessed [January, 2019].

Vano, J.A., Nijssen, B., Lettenmaier, D.P. (2015). Seasonal hydrologic responses to climate change in the Pacific Northwest. *Water Resources Research, 51,* 1959-1976.

Watson, E., & Luckman, B.H. (2005). An exploration of the controls of pre-instrumental streamflow using multiple tree-ring proxies. *Dendrochronologia, 22,* 225-234.

Wiley, M.W., Palmer, R.N. (2008). Estimating the Impacts and Uncertainty of Climate Change on a Municipal Water Supply System. *Journal of Water Resources Planning and Management, 134(3),* 239-246.

Woodhouse, C.A., Gray, S.T., Meko, D.M. (2006). Updated streamflow reconstructions for the Upper Colorado River Basin. *Water Resources Research, 42,* W05415.

Woodward, A., Silsbee, D.G., Schreiner, E.G., Means, J.E. (1994). Influence of climate on radial growth and cone production in subalpine fir (*Abies lasiocarpa*) and mountain hemlock (*Tsuga mertensiana*). *Canadian Journal of Forest Research, 24,* 1133-1143.

7.0 Tables

Table 1. Variance described by principal components of ring-width chronologies.

	PC1	PC2	PC3
Total width	0.86	0.09	0.05
Earlywood	0.83	0.11	0.06
Latewood	0.77	0.14	0.09
Adjusted latewood	0.66	0.21	0.13

Table 2. Summary of tree core samples, crossdating statistics, and prewhitened residual total width chronologies. *The Heather Meadows site contains 32 cores from 18 trees collected by this study in 2019, and 14 cores from 14 trees collected by A.G. Bunn in 2007.

	Heather Meadows	Grouse Ridge	Canyon Ridge	NFN Basin Regional
Number of cores	46*	41	40	127
Number of trees	32*	20	20	72
Interval (yr)	1432-2018	1545-2018	1430-2018	1430-2018
Mean core length (yrs)	298	375	301	324
Series intercorrelation	0.547	0.617	0.690	0.591
Mean sensitivity	0.241	0.227	0.264	0.243

Table 3. Correlations between all regional ring-width and PC chronologies. Values are Pearson's R. Cells highlighted with a bold border represent correlations between respective seasonal pairings of ring-width and PC chronologies. TW = total width, EW = earlywood, LW = raw (non-adjusted) latewood, LWa = adjusted latewood, RW = ring-width chronology, PC = principal component chronology.

	TW RW	**EW RW**	**LW RW**	**LWa RW**	**TW PC**	**EW PC**	**LW PC**
TW RW	-						
EW RW	0.97	-					
LW RW	0.88	0.78	-				
LWa RW	0.28	0.09	0.68	-			
TW PC	0.99	0.97	0.88	0.28	-		
EW PC	0.98	0.98	0.81	0.16	0.98	-	
LW PC	0.88	0.77	0.99	0.69	0.88	0.82	-
LWa PC	0.27	0.08	0.68	0.99	0.28	0.15	0.69

Table 4. Correlations between ring-width chronologies and monthly climate variables (Pearson's R). Bold text indicates significant correlations at a 95% confidence level. A "-" symbol next to a month indicates climatic/hydrologic data from the previous year. TW = total ring-width chronology, EW = earlywood width chronology, LW = raw (non-adjusted) latewood width chronology, LWa = adjusted latewood width chronology.

	Average Temperature				**Maximum Temperature**				**Minimum Temperature**			
	TW	EW	LW	LWa	TW	EW	LW	LWa	TW	EW	LW	LWa
-Jun	-0.18	-0.17	-0.15	-0.06	-0.14	-0.13	-0.11	-0.04	-0.16	-0.17	-0.15	-0.06
-Jul	**-0.51**	**-0.46**	**-0.51**	**-0.30**	**-0.47**	**-0.41**	**-0.48**	**-0.30**	**-0.35**	**-0.34**	**-0.34**	-0.17
-Aug	-0.10	-0.07	**-0.21**	**-0.24**	-0.13	-0.07	**-0.25**	**-0.32**	-0.01	-0.02	-0.03	-0.01
-Sep	0.06	0.07	0.02	-0.06	0.09	0.09	0.06	-0.02	-0.01	0.00	-0.05	-0.09
-Oct	0.10	0.16	-0.05	**-0.24**	0.15	**0.21**	-0.01	**-0.22**	0.00	0.05	-0.09	-0.19
-Nov	0.15	0.16	0.06	-0.08	0.15	0.17	0.06	-0.09	0.13	0.15	0.06	-0.06
-Dec	0.14	0.16	0.08	-0.03	0.15	0.16	0.09	-0.02	0.13	0.15	0.06	-0.04
Jan	**0.20**	**0.19**	**0.21**	0.11	**0.20**	**0.21**	**0.21**	0.10	**0.19**	0.18	**0.21**	0.13
Feb	0.01	0.03	-0.03	-0.06	0.02	0.04	-0.04	-0.08	0.00	0.01	-0.02	-0.02
Mar	**0.20**	**0.23**	0.11	-0.08	**0.23**	**0.25**	0.16	-0.03	0.13	0.17	0.04	-0.12
Apr	**0.22**	**0.23**	**0.21**	0.10	**0.26**	**0.26**	**0.26**	0.14	0.12	0.13	0.10	0.02
May	0.11	0.13	0.06	-0.06	0.15	0.16	0.11	-0.02	0.02	0.04	-0.03	-0.08
Jun	**0.19**	**0.19**	0.15	0.03	**0.26**	**0.25**	**0.26**	0.14	0.01	0.03	-0.07	-0.14
Jul	0.19	0.17	**0.24**	0.17	**0.22**	0.19	**0.31**	**0.25**	0.06	0.06	0.03	-0.01
Aug	-0.04	-0.08	0.09	**0.21**	0.04	-0.01	**0.20**	**0.32**	-0.13	-0.12	-0.11	-0.04
Sep	0.03	0.04	-0.02	-0.07	0.04	0.03	0.00	-0.02	0.01	0.04	-0.05	-0.11

Table continues on next page

	Total Precipitation				Average Streamflow				Snowpack (SWE)			
	TW	EW	LW	LWa	TW	EW	LW	LWa	TW	EW	LW	LWa
-Jun	0.10	0.10	0.05	-0.02	0.15	0.11	0.19	0.17	**0.37**	**0.32**	**0.36**	**0.25**
-Jul	**0.27**	**0.23**	**0.28**	**0.20**	**0.22**	0.16	**0.27**	**0.25**	**0.38**	**0.32**	**0.37**	**0.28**
-Aug	0.13	0.06	**0.29**	**0.39**	**0.31**	**0.24**	**0.33**	**0.26**	**0.28**	0.21	**0.37**	**0.37**
-Sep	-0.08	-0.08	-0.04	0.02	0.04	-0.01	0.10	0.17	NA	NA	NA	NA
-Oct	**-0.23**	**-0.24**	-0.17	-0.02	-0.12	-0.15	0.01	0.17	**-0.34**	**-0.36**	-0.23	-0.01
-Nov	-0.05	-0.10	0.06	**0.20**	-0.16	**-0.22**	-0.02	0.19	**-0.27**	**-0.29**	-0.16	0.03
-Dec	-0.09	-0.08	-0.11	-0.08	-0.05	-0.04	-0.01	0.03	**-0.48**	**-0.48**	**-0.37**	-0.11
Jan	-0.05	-0.08	-0.01	0.09	-0.12	-0.13	-0.11	-0.03	**-0.58**	**-0.61**	**-0.45**	-0.10
Feb	-0.15	**-0.19**	0.00	0.18	-0.12	-0.13	-0.05	0.06	**-0.51**	**-0.56**	**-0.34**	0.02
Mar	**-0.26**	**-0.27**	**-0.23**	-0.07	-0.04	-0.04	-0.04	-0.03	**-0.52**	**-0.57**	**-0.34**	0.03
Apr	**-0.23**	**-0.21**	**-0.25**	-0.17	0.06	0.05	0.07	0.08	**-0.55**	**-0.61**	**-0.37**	0.01
May	0.06	0.06	0.07	0.05	-0.15	-0.15	-0.14	-0.07	**-0.56**	**-0.61**	**-0.37**	0.02
Jun	**-0.22**	**-0.22**	-0.18	-0.03	-0.17	**-0.24**	-0.05	0.15	**-0.57**	**-0.63**	**-0.39**	0.00
Jul	**-0.25**	**-0.22**	**-0.28**	**-0.19**	**-0.41**	**-0.49**	**-0.25**	0.12	**-0.58**	**-0.62**	**-0.42**	-0.04
Aug	-0.06	-0.03	-0.14	**-0.19**	**-0.51**	**-0.56**	**-0.37**	0.01	**-0.37**	**-0.32**	**-0.44**	**-0.37**
Sep	-0.01	-.00	-0.02	-0.03	**-0.35**	**-0.36**	**-0.29**	-0.07	NA	NA	NA	NA

Table 5. Summary statistics of cross-validation (rolling forecasting origin with 80 samples, non-fixed window, minimum sample size of 36, withholding 6 values from each sample) and full calibration period models considered for reconstruction of average August streamflow. *RW = regional ring-width chronology, PC = principal component chronology. **Chosen model.

	Rolling Forecasting Origin Cross-Validation			Full Calibration Period		
Model Predictors*	**Adj. R-sq**	**RMSE**	**MAE**	**Adj. R-sq**	**RSE**	**AIC**
Total RW	0.3501	198.12	165.61	0.2555	199.5	1078.32
Earlywood RW	0.4090	189.78	157.08	0.3026	193.1	1073.10
Earlywood + Adjusted Latewood RW	0.4230	188.06	155.52	0.3041	192.9	1073.89
Earlywood + Adjusted Latewood (T+1) RW **	0.4275	191.33	159.33	0.3176	191.0	1072.33
Total Width PC	0.3452	199.22	166.03	0.2533	199.8	1078.56
Earlywood PC	0.3711	195.77	163.01	0.2794	196.3	1075.72
Earlywood + Adjusted Latewood PC	0.4006	191.23	158.53	0.2928	194.4	1075.18
Earlywood + Adjusted Latewood (T+1) PC	0.4000	196.52	164.27	0.2942	194.2	1075.02

8.0 Figures

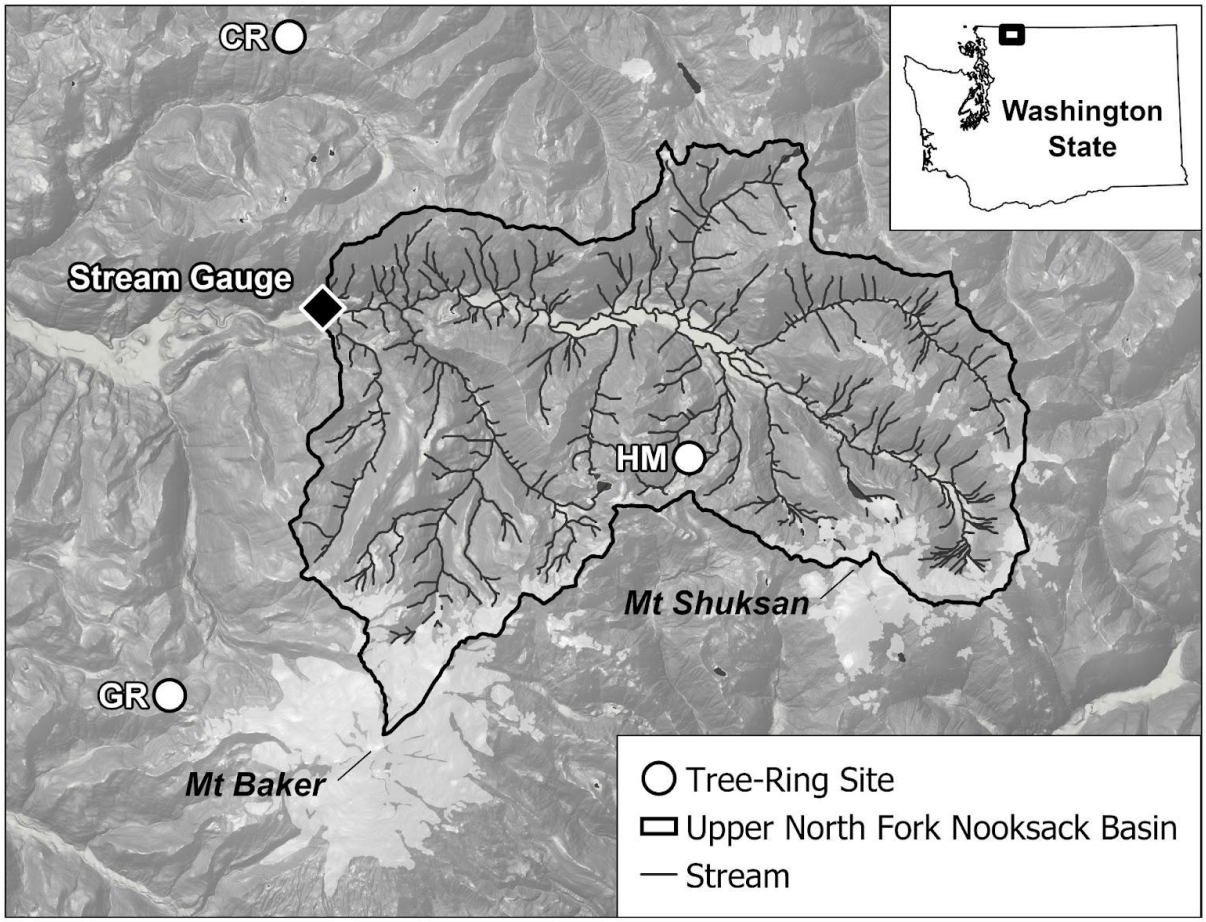

Figure 1. Map of study sites. Tree-ring data collection sites are indicated with white circles, where CR = Canyon Ridge, GR = Grouse Ridge, and HM = Heather Meadows. USGS stream gauge no.12205000, "NF Nooksack River below Cascade Creek near Glacier, WA" is indicated with a black diamond. The upper North Fork Nooksack basin is indicated with a bold outline and represents the area which drains to the stream gauge. The Canyon Ridge site is located at 48.986°N, -121.888°W at approximately 4,500 ft above sea level. The Grouse Ridge site is located at 48.794°N, -121.912°W at approximately 4,900 ft above sea level. The Heather Meadows site is located at 48.858°N, -121.683°W at approximately 4,350 ft above sea level. The stream gauge is located at 48.906°N, -121.843°W at approximately 1,280 ft above sea level.

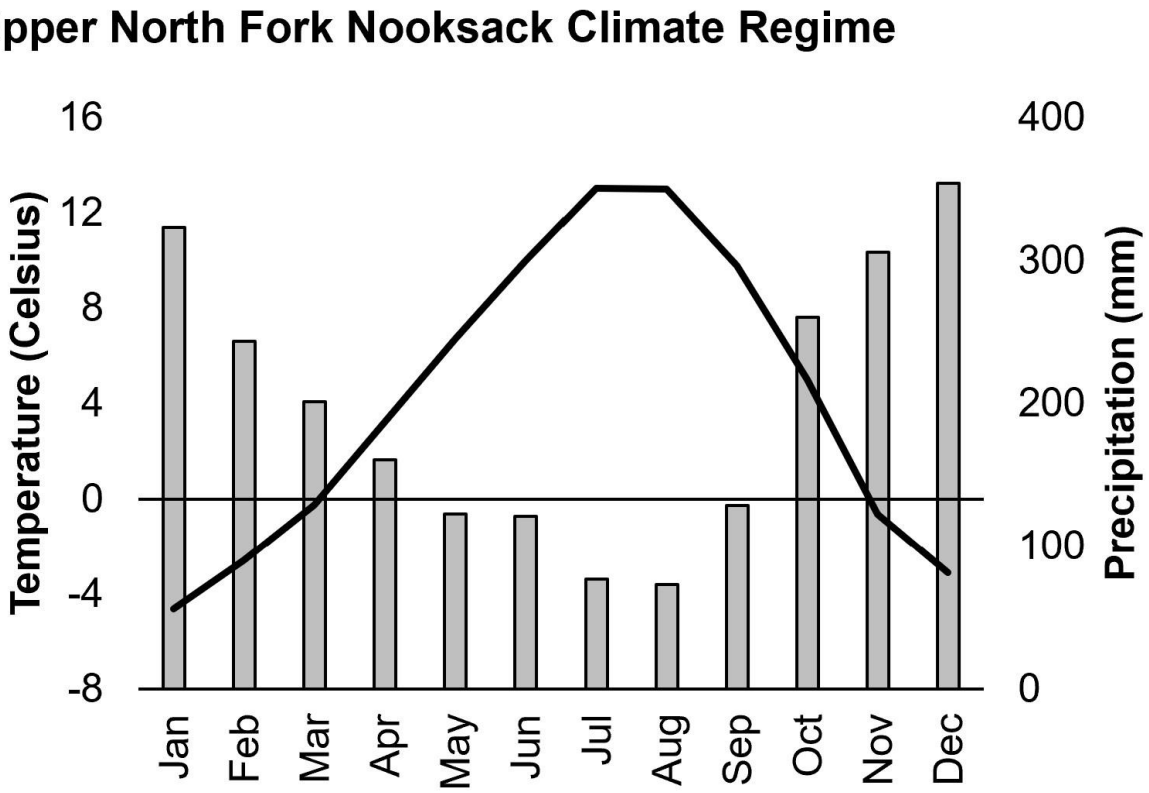

Figure 2. Monthly climate regime of the upper North Fork Nooksack basin from 1901-2009. Average monthly temperature is plotted as a line on the left axis, total monthly precipitation is plotted as columns on the right axis. Data is monthly PRISM data encompassing the upper North Fork Nooksack basin area.

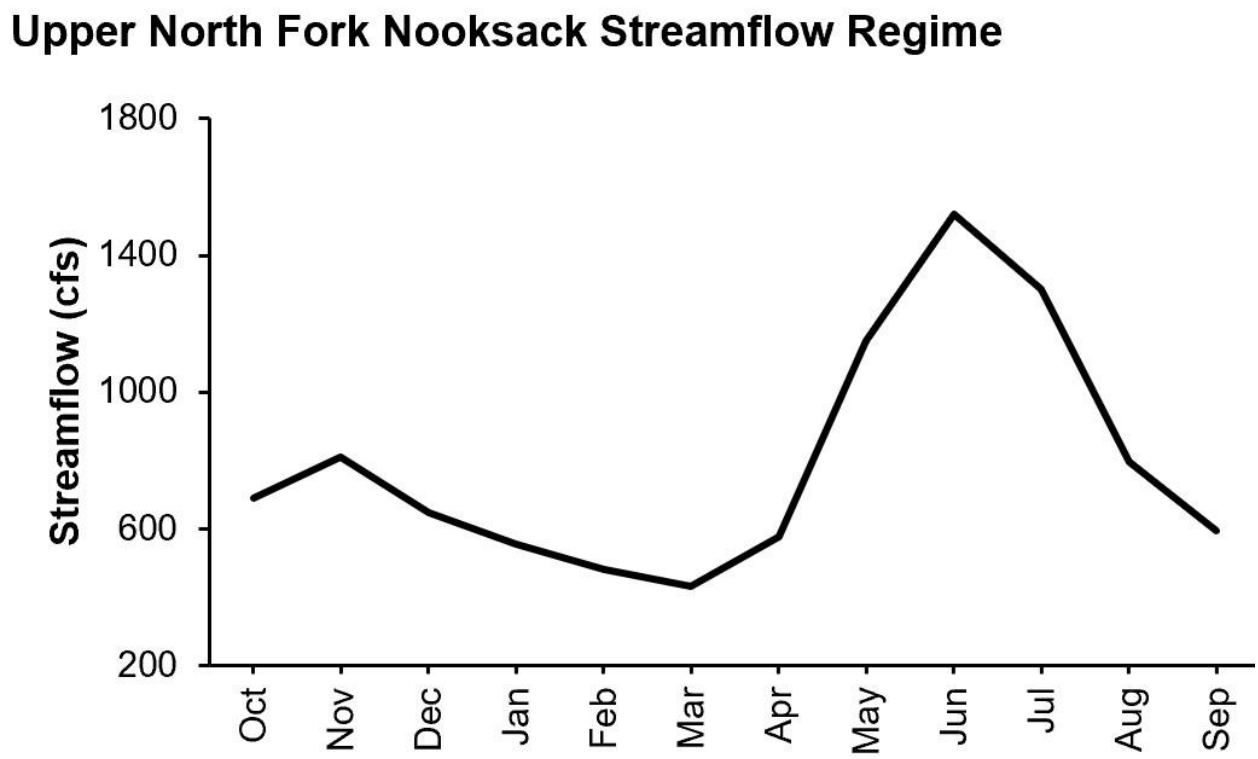

Figure 3. Monthly streamflow regime of the upper North Fork Nooksack River from 1938-2018 at USGS stream gauge no. 12205000, "NF Nooksack River below Cascade Creek near Glacier, WA".

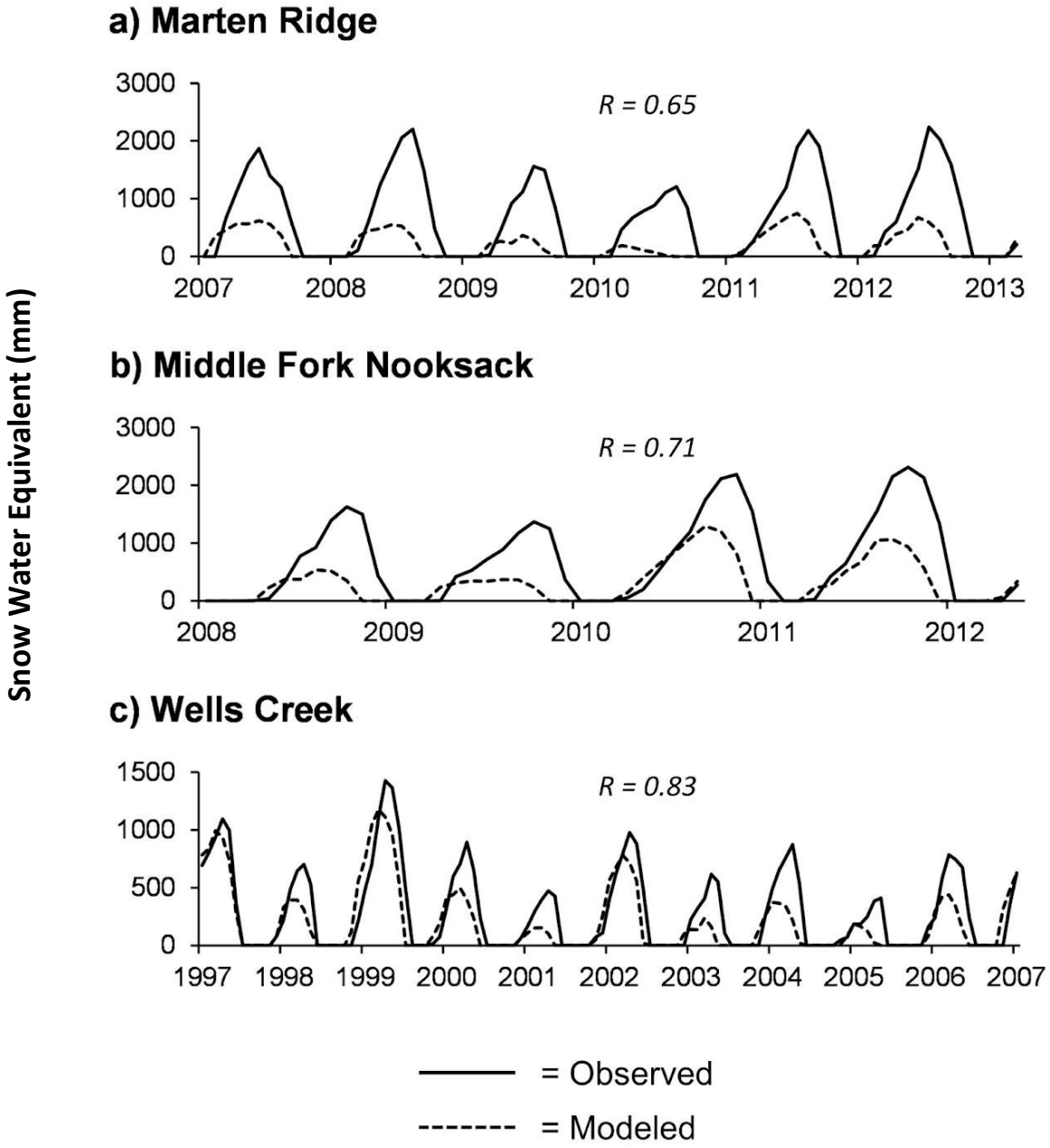

Figure 4. Observed and modeled data (solid and dashed lines, respectively) from the three Snowpack Telemetry Network (SNOTEL) sites nearest to the upper North Fork Nooksack Basin. These sites are located at a) Marten Ridge (elevation = 1,073m), b) Middle Fork Nooksack (elevation = 1,515m), c) Wells Creek (elevation = 1,228m).

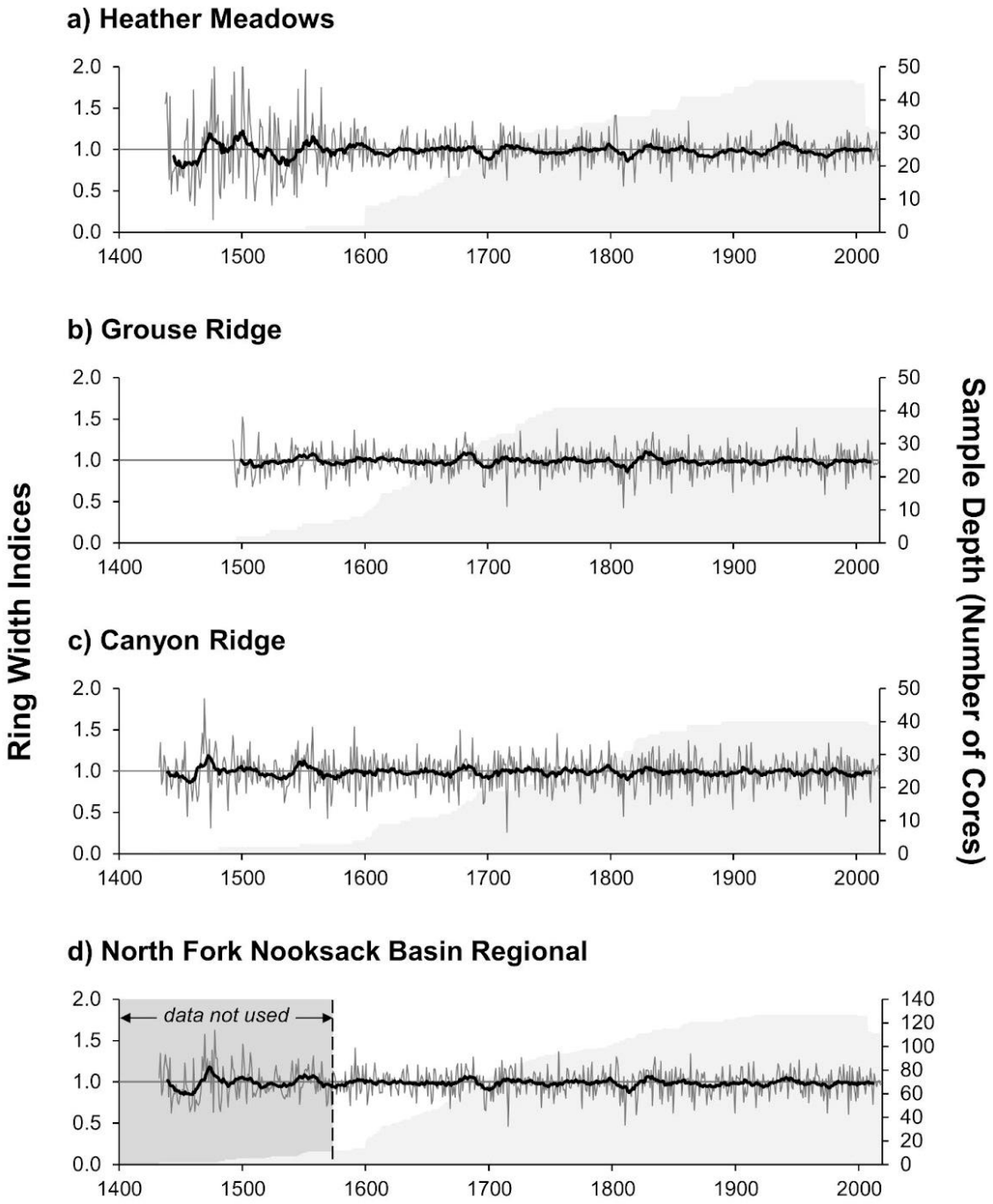

Figure 5. Pre-whitened total width residual chronologies produced by this study. Individual series from site chronologies (panels a, b, and c) were combined to make the North Fork Nooksack Basin Regional total width chronology. Chronologies are plotted with a 15-year rolling mean to emphasize trends. The gray box in panel d) indicates where the regional chronology was truncated prior to further analyses (1574, based on a subsample signal strength (SSS) > 0.85). The sample depth, or number of cores contributing to a chronology in each year, is indicated on the secondary axes of each chart.

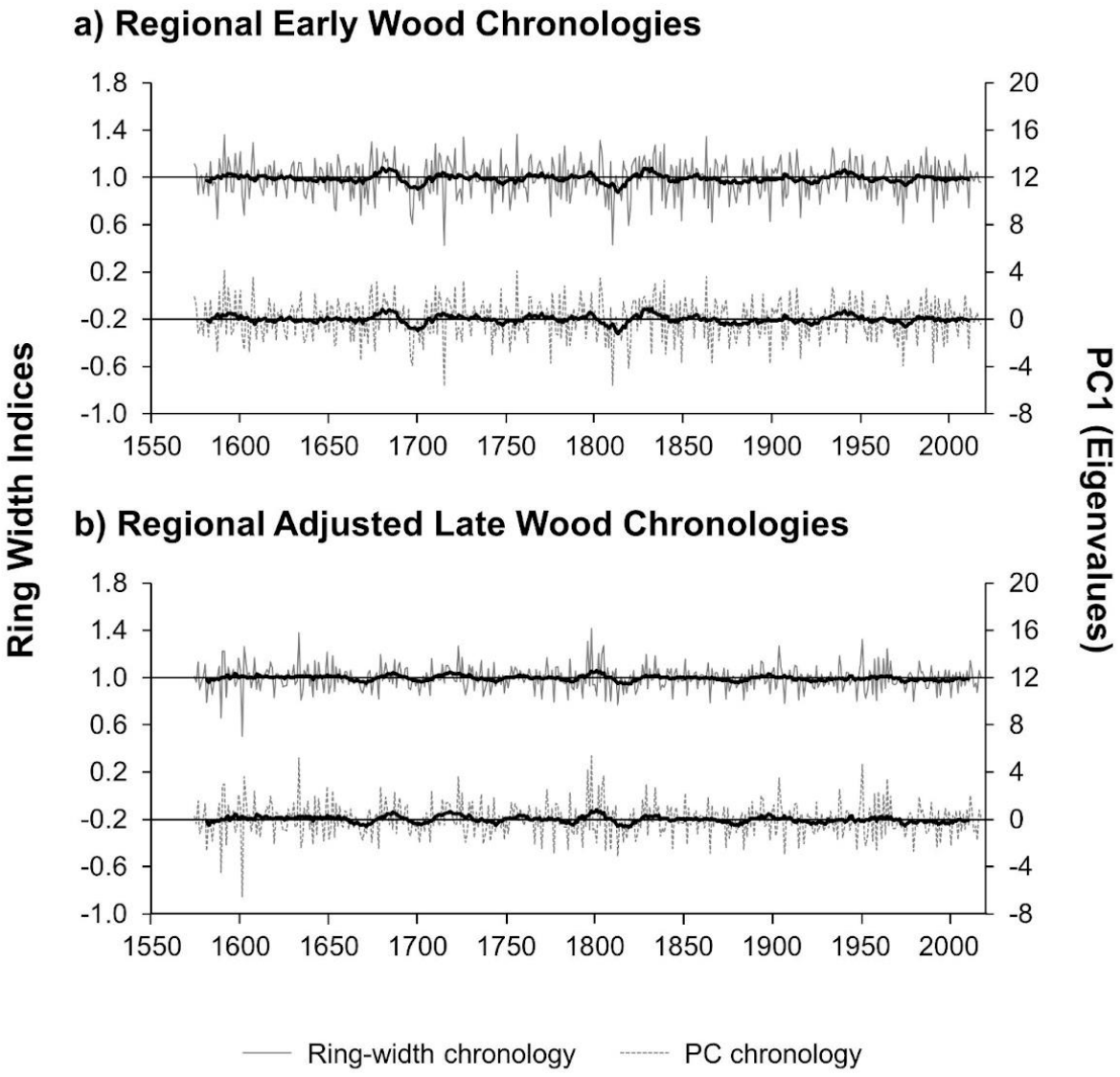

Figure 6. Regional earlywood and adjusted latewood residual and principal component (PC) chronologies. Regional residual chronologies were created with individual series from the three site locations (Heather Meadows, Grouse Ridge, and Canyon Ridge). PC chronologies were created with Principal Component Analyses where inputs were the corresponding earlywood or adjusted latewood residual chronologies from each of the three site locations. Chronologies were truncated to 1574-2018 based on an SSS > 0.85. Chronologies were plotted with a 15-year rolling mean (bold line) to emphasize trends.

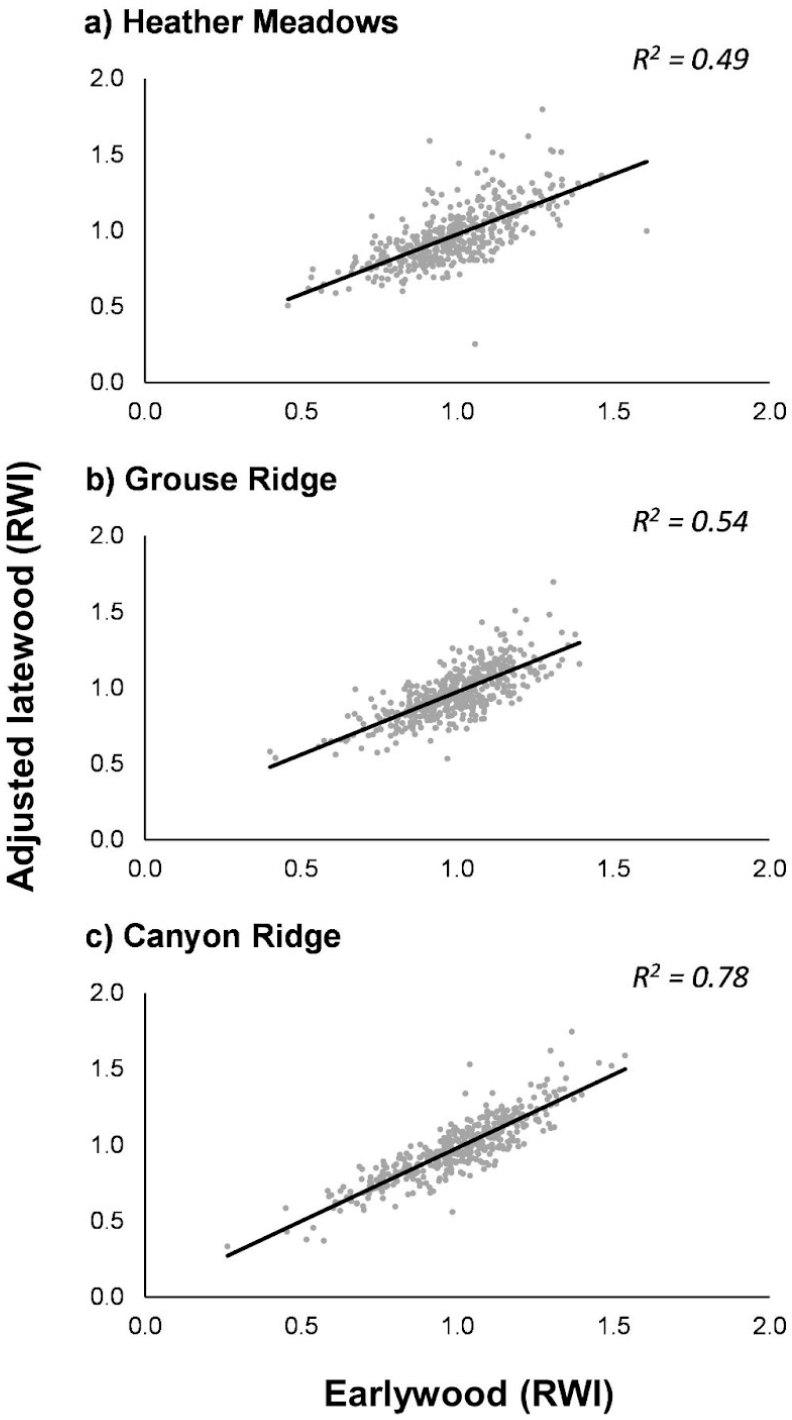

Figure 7. The residuals of linear models with site latewood ring-width chronologies as dependent variables and site earlywood ring-width chronologies as independent variables made up site adjusted latewood ring-width chronologies. A regional adjusted latewood ring-width chronology was later calculated by averaging the site adjusted latewood chronologies together.

a)

Monthly Average Streamflow \ Monthly Average Temperature	Jan	Feb	Mar	Apr	May	Jun	Jul	Aug	Sep	Oct	Nov	Dec
Jan	**0.48**	**0.36**	0.20	0.06	-0.07	0.11	0.16	0.24	-0.03	-0.11	0.07	0.04
Feb	0.07	**0.54**	0.12	-0.01	0.08	0.07	0.06	0.21	-0.07	-0.01	0.06	-0.05
Mar	0.09	0.16	**0.47**	0.07	0.27	0.15	0.11	0.29	0.03	0.06	0.08	-0.05
Apr	-0.06	-0.08	0.2	**0.62**	0.09	-0.02	0.08	0.13	0.03	0.11	0.13	0.14
May	-0.20	-0.27	0.01	0.02	**0.67**	-0.06	-0.11	0.04	0.12	-0.12	0.20	0.05
Jun	-0.06	-0.30	**-0.42**	**-0.47**	-0.27	0.23	-0.10	-0.07	-0.11	**-0.41**	-0.11	-0.19
Jul	-0.08	-0.12	**-0.45**	**-0.50**	**-0.34**	**-0.38**	-0.19	-0.15	-0.10	**-0.39**	0.12	-0.10
Aug	-0.08	-0.03	**-0.37**	**-0.47**	**-0.44**	**-0.36**	**-0.40**	0.00	-0.09	-0.27	0.26	0.01
Sep	-0.22	0.01	-0.10	-0.26	-0.17	0.04	-0.15	-0.20	-0.14	-0.13	0.10	0.04
Oct	0.10	-0.05	0.01	-0.14	-0.07	0.06	0.15	0.06	0.01	0.00	-0.18	0.03
Nov	0.19	-0.08	-0.05	-0.02	-0.09	-0.06	0.08	0.08	0.08	-0.26	**0.32**	-0.11
Dec	-0.06	-0.11	0.10	0.16	0.08	-0.05	0.12	0.09	0.18	0.06	0.17	**0.49**

b)

Monthly Average Streamflow \ Monthly Maximum Temperature	Jan	Feb	Mar	Apr	May	Jun	Jul	Aug	Sep	Oct	Nov	Dec
Jan	**0.45**	**0.34**	0.11	-0.07	-0.15	0.08	0.10	0.22	-0.06	-0.15	0.01	0.03
Feb	0.06	**0.50**	0.11	-0.06	0.03	0.03	0.00	0.15	-0.07	-0.04	-0.02	-0.07
Mar	0.09	0.12	**0.34**	-0.07	0.20	0.14	0.01	0.25	-0.03	0.04	0.02	-0.08
Apr	-0.08	-0.04	0.21	**0.51**	0.01	0.01	0.06	0.14	0.01	0.06	0.13	0.15
May	-0.19	-0.26	0.00	0.03	**0.63**	-0.10	-0.09	0.09	0.12	-0.06	0.23	0.04
Jun	-0.07	**-0.35**	**-0.47**	**-0.42**	-0.22	0.19	-0.07	0.00	0.00	**-0.31**	-0.08	-0.17
Jul	-0.10	-0.21	**-0.50**	**-0.42**	-0.26	**-0.38**	-0.16	-0.14	-0.01	**-0.32**	0.11	-0.10
Aug	-0.09	-0.10	**-0.40**	**-0.41**	**-0.41**	**-0.35**	**-0.39**	-0.13	-0.04	-0.16	0.22	0.00
Sep	-0.25	-0.03	-0.14	-0.24	-0.15	0.00	-0.14	-0.28	-0.27	-0.10	0.13	0.04
Oct	0.10	-0.04	0.00	-0.20	-0.06	0.03	0.19	0.09	-0.03	-0.27	-0.17	0.06
Nov	0.19	-0.07	-0.05	0.00	-0.09	-0.13	0.02	-0.06	0.07	**-0.32**	0.23	-0.09
Dec	-0.07	-0.11	0.08	0.21	0.08	-0.09	0.09	0.11	0.17	-0.05	0.16	**0.48**

Figure continues on next page

c)

Monthly Average Streamflow	Monthly Minimum Temperature											
	Jan	Feb	Mar	Apr	May	Jun	Jul	Aug	Sep	Oct	Nov	Dec
Jan	**0.50**	**0.34**	0.29	0.23	0.09	0.14	0.22	0.15	0.04	0.00	0.12	0.05
Feb	0.08	**0.53**	0.11	0.07	0.14	0.13	0.15	0.22	-0.05	0.03	0.14	-0.03
Mar	0.09	0.19	**0.57**	0.26	**0.31**	0.14	0.24	0.22	0.13	0.07	0.13	-0.03
Apr	-0.04	-0.12	0.17	**0.63**	0.21	-0.07	0.08	0.05	0.06	0.14	0.13	0.13
May	-0.20	-0.26	0.02	-0.01	**0.56**	0.04	-0.12	-0.07	0.07	-0.16	0.16	0.05
Jun	-0.05	-0.23	**-0.30**	**-0.44**	-0.28	0.24	-0.13	-0.15	-0.26	**-0.40**	-0.14	-0.20
Jul	-0.06	-0.03	**-0.33**	**-0.51**	**-0.38**	-0.27	-0.18	-0.08	-0.24	**-0.34**	0.12	-0.09
Aug	-0.08	0.05	-0.27	**-0.46**	**-0.37**	-0.28	-0.29	0.23	-0.14	**-0.32**	0.28	0.02
Sep	-0.19	0.05	-0.03	-0.23	-0.16	0.09	-0.11	0.05	0.16	-0.13	0.07	0.05
Oct	0.10	-0.06	0.02	-0.03	-0.07	0.10	0.03	-0.01	0.07	**0.38**	-0.19	0.00
Nov	0.20	-0.09	-0.04	-0.05	-0.07	0.10	0.16	0.29	0.08	-0.07	**0.39**	-0.13
Dec	-0.06	-0.10	0.11	0.05	0.06	0.05	0.14	0.01	0.12	0.19	0.16	**0.50**

d)

Monthly Average Streamflow	Monthly Total Precipitation											
	Jan	Feb	Mar	Apr	May	Jun	Jul	Aug	Sep	Oct	Nov	Dec
Jan	**0.56**	-0.01	0.17	0.21	0.28	0.06	-0.01	-0.02	0.14	0.00	0.24	-0.06
Feb	0.25	**0.31**	-0.07	0.07	0.02	-0.02	0.05	0.09	-0.01	-0.02	0.26	-0.04
Mar	0.27	0.22	**0.33**	0.14	0.07	0.00	**0.32**	-0.12	0.01	-0.18	-0.04	0.12
Apr	0.01	-0.05	0.09	0.30	0.13	0.09	0.00	-0.20	0.01	-0.06	-0.04	-0.13
May	0.05	0.06	0.17	-0.04	-0.13	0.20	0.10	-0.12	0.02	-0.13	-0.25	-0.03
Jun	**0.34**	0.28	**0.34**	0.03	-0.03	0.07	0.11	0.07	0.08	0.12	0.03	-0.03
Jul	**0.49**	**0.35**	**0.34**	0.01	-0.10	**0.32**	0.18	0.19	-0.09	0.05	0.02	0.16
Aug	**0.33**	**0.32**	0.18	-0.09	0.02	0.22	0.25	**0.38**	-0.11	-0.13	0.00	0.08
Sep	0.12	0.14	0.21	0.01	-0.02	0.09	0.04	**0.43**	**0.51**	-0.06	-0.07	0.01
Oct	0.12	0.01	0.19	0.09	-0.02	-0.10	-0.14	0.08	0.14	**0.67**	0.04	-0.04
Nov	0.16	-0.07	-0.13	0.05	0.00	0.07	0.03	0.24	-0.05	0.26	**0.69**	-0.07
Dec	-0.06	-0.06	0.02	-0.05	-0.03	-0.07	-0.03	0.03	-0.13	0.17	0.14	**0.64**

Figure continues on next page

e)

Monthly Average Streamflow	Monthly Total Snowpack: Jan	Feb	Mar	Apr	May	Jun	Jul	Aug	Sep	Oct	Nov	Dec
Jan	0.01	-0.09	-0.10	-0.09	-0.06	0.01	0.11	-0.08	NA	-0.09	0.07	0.02
Feb	0.16	0.12	0.06	0.06	0.06	0.07	0.07	-0.03	NA	-0.11	0.01	0.02
Mar	0.13	0.13	0.09	0.10	0.09	0.10	0.14	-0.14	NA	-0.02	-0.09	0.08
Apr	-0.11	-0.06	-0.06	-0.11	-0.10	-0.08	-0.09	-0.28	NA	0.09	-0.04	-0.10
May	0.18	0.23	0.25	0.22	0.16	0.17	0.09	0.01	NA	-0.03	-0.27	-0.25
Jun	0.24	**0.41**	**0.52**	**0.54**	**0.55**	**0.50**	**0.45**	0.04	NA	0.22	0.05	0.03
Jul	**0.41**	**0.60**	**0.70**	**0.73**	**0.75**	**0.79**	**0.78**	**0.38**	NA	0.11	-0.08	0.04
Aug	**0.43**	**0.48**	**0.53**	**0.57**	**0.61**	**0.66**	**0.73**	**0.42**	NA	-0.09	-0.17	-0.16
Sep	**0.39**	0.29	0.30	**0.33**	**0.34**	**0.34**	**0.35**	0.27	NA	-0.10	-0.19	-0.22
Oct	-0.13	-0.08	0.01	0.04	0.05	0.05	0.01	-0.05	NA	**0.38**	0.09	-0.02
Nov	-0.12	-0.06	-0.05	-0.05	-0.03	-0.02	0.00	-0.01	NA	**0.47**	**0.35**	0.19
Dec	-0.09	-0.10	-0.10	-0.11	-0.11	-0.08	-0.11	-0.06	NA	0.12	0.02	0.10

Significant (99%) negative correlation	Significant (95%) negative correlation	Non-significant negative correlation	Non-significant positive correlation	Significant (95%) positive correlation	**Significant (99%) positive correlation**

Figure 8. Correlations between basin-scale climate variables and monthly average streamflow. a) monthly average temperature, b) monthly maximum temperature, c) monthly minimum temperature, d) monthly total precipitation, e) monthly snowpack (SWE). Warm colors denote positive correlation and cool colors denote negative correlation. More saturated colors denote significant correlations at a 95% confidence level and bold text denotes significant correlations at a 99% confidence interval. Correlation coefficients are Pearson's R. August monthly average streamflow is highlighted with a box to indicate the subject of the reconstruction performed later in this study.

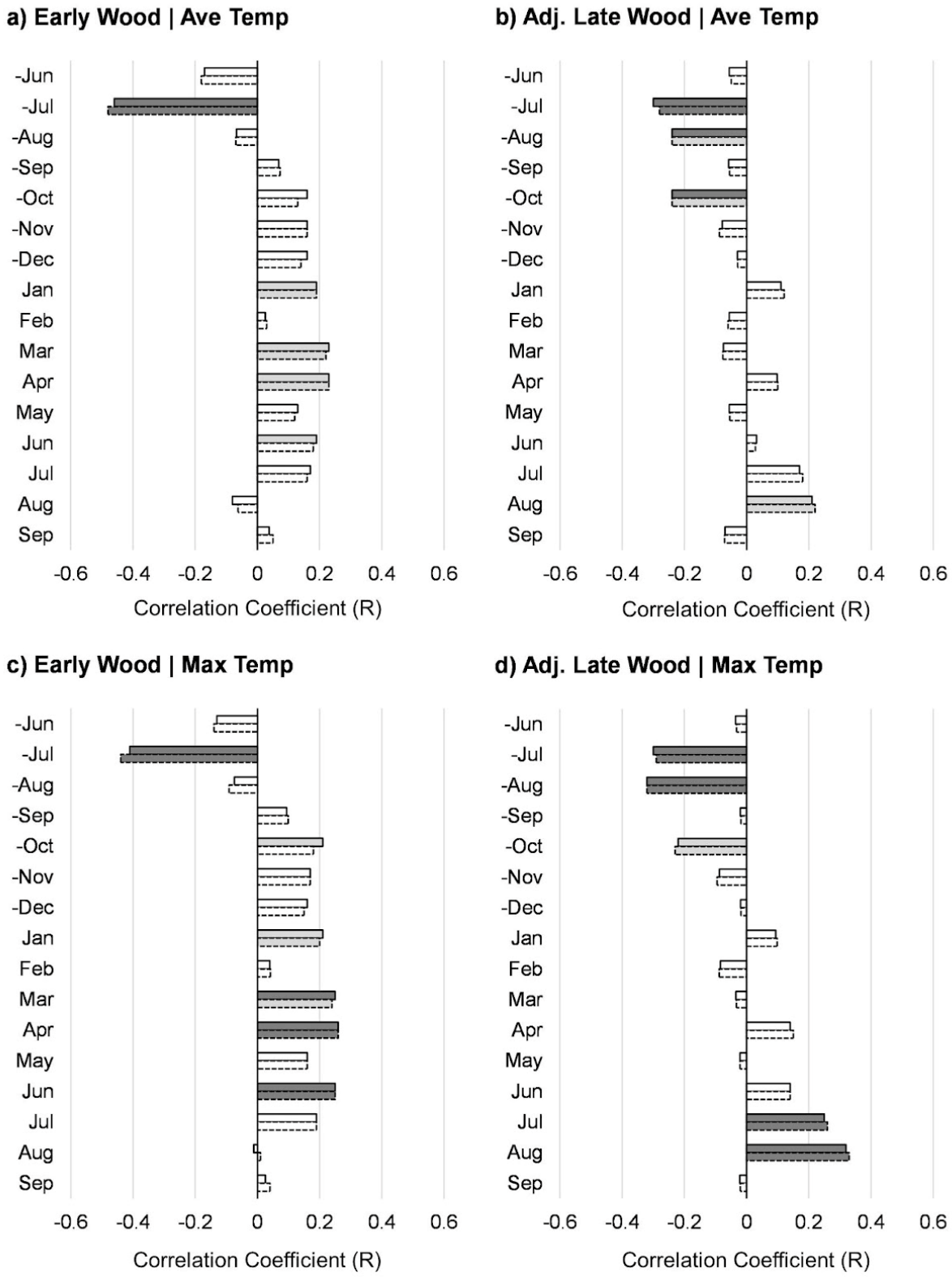

Figure continues on next page

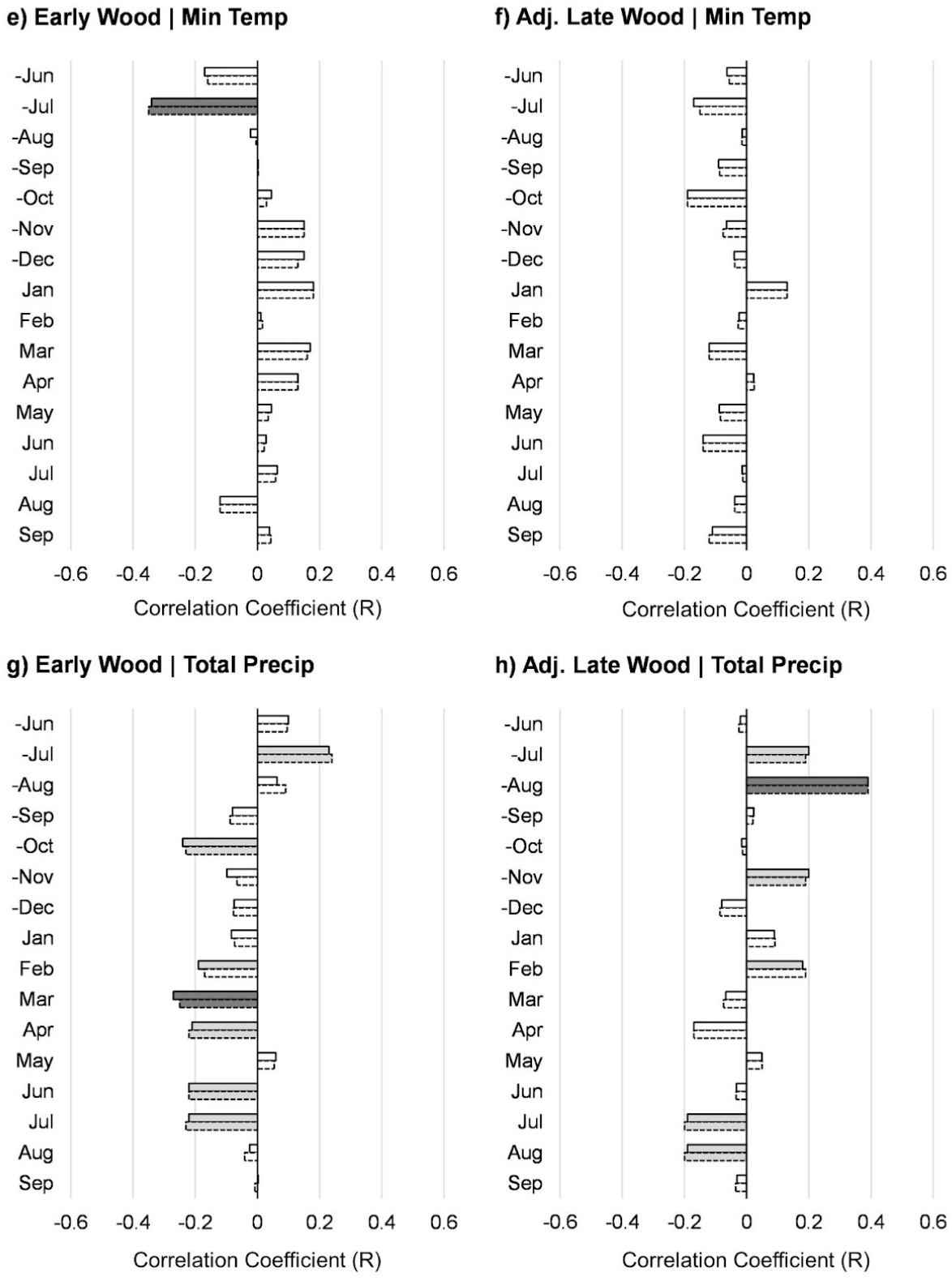

Figure continues on next page

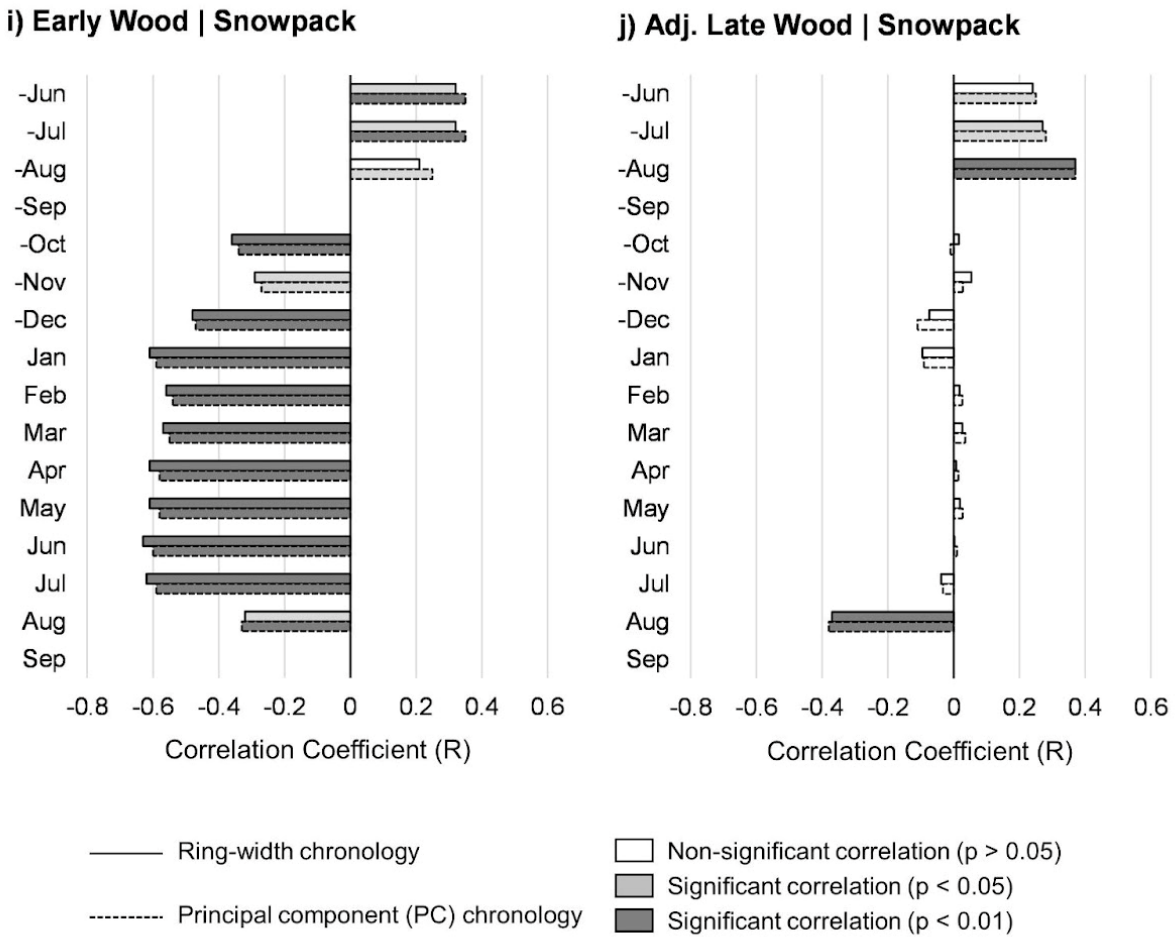

Figure 9. Correlations between basin-scale climate variables (monthly average temperature, monthly maximum temperature, monthly minimum temperature, monthly total precipitation) and tree-ring chronologies (regional earlywood ring-width, earlywood PC, regional adjusted latewood ring-width, adjusted latewood PC). a) earlywood chronologies vs. monthly average temperature, b) adjusted latewood chronologies vs. monthly average temperature, c) earlywood chronologies vs. monthly maximum temperature, d) adjusted latewood chronologies vs. monthly maximum temperature, e) earlywood chronologies vs. monthly minimum temperature, f) adjusted latewood chronologies vs. monthly minimum temperature, g) earlywood chronologies vs. monthly total precipitation, h) adjusted latewood chronologies vs monthly total precipitation, i) earlywood vs. monthly snowpack, j) adjusted latewood vs. monthly snowpack. Solid-outlined bars denote ring-width chronologies, dashed-outlined bars denote PC chronologies. Light gray bars denote significant correlation at a 95% confidence level, dark gray bars denote significant correlation at a 99% confidence level. Correlation coefficients are Pearson's R.

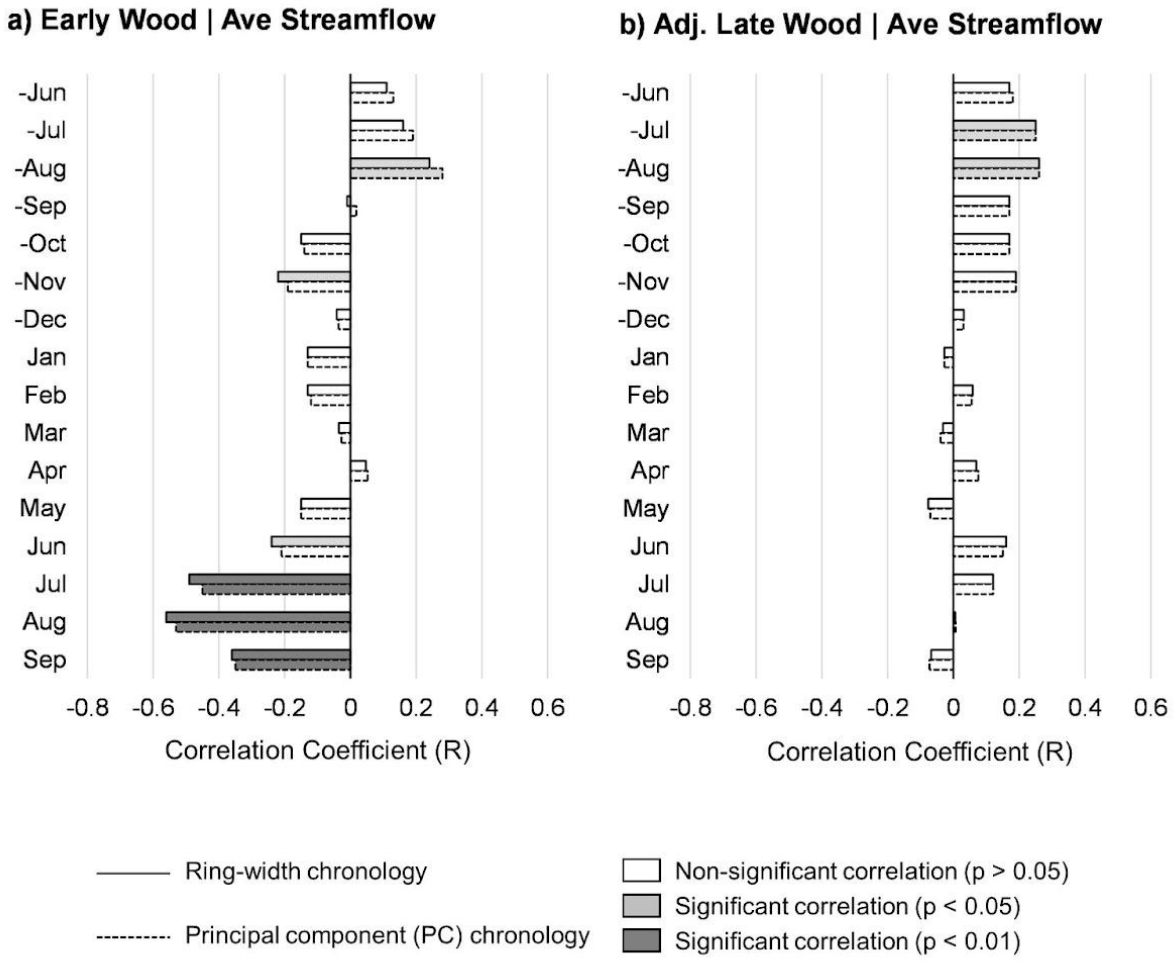

Figure 10. Correlations between monthly average streamflow and tree-ring chronologies (regional earlywood ring-width, earlywood PC, regional adjusted latewood ring-width, adjusted latewood PC). a) earlywood vs. monthly average streamflow, b) adjusted latewood vs. monthly average streamflow. Solid-outlined bars denote ring-width chronologies, dashed-outlined bars denote PC chronologies. Light gray bars denote significant correlation at a 95% confidence level, dark gray bars denote significant correlation at a 99% confidence level. Correlation coefficients are Pearson's R.

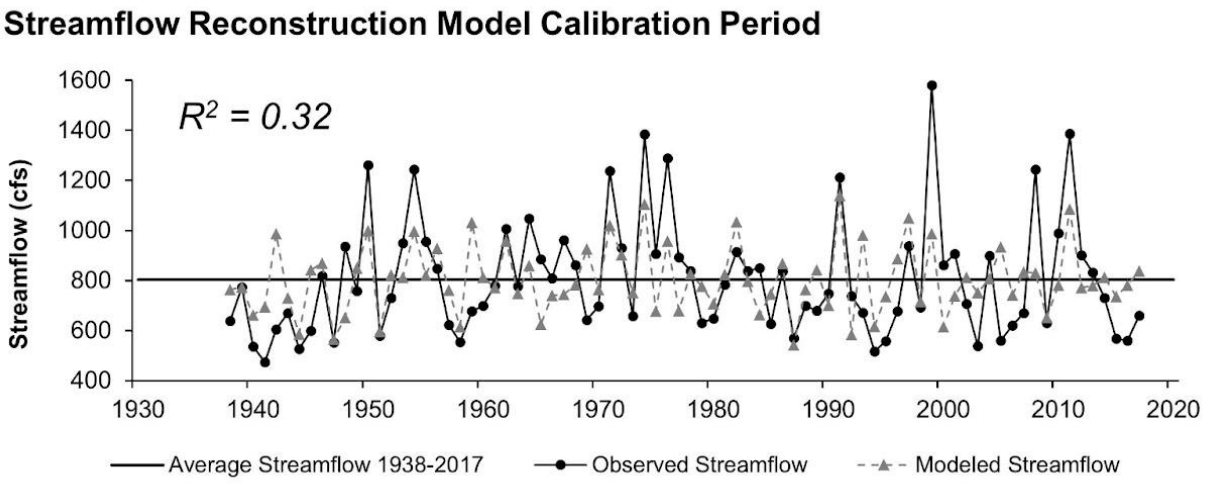

Figure 11. Observed and modeled average August streamflow data during the model calibration period (1938-2017).The horizontal line indicates the average of observed August streamflow values (802.5 cfs).

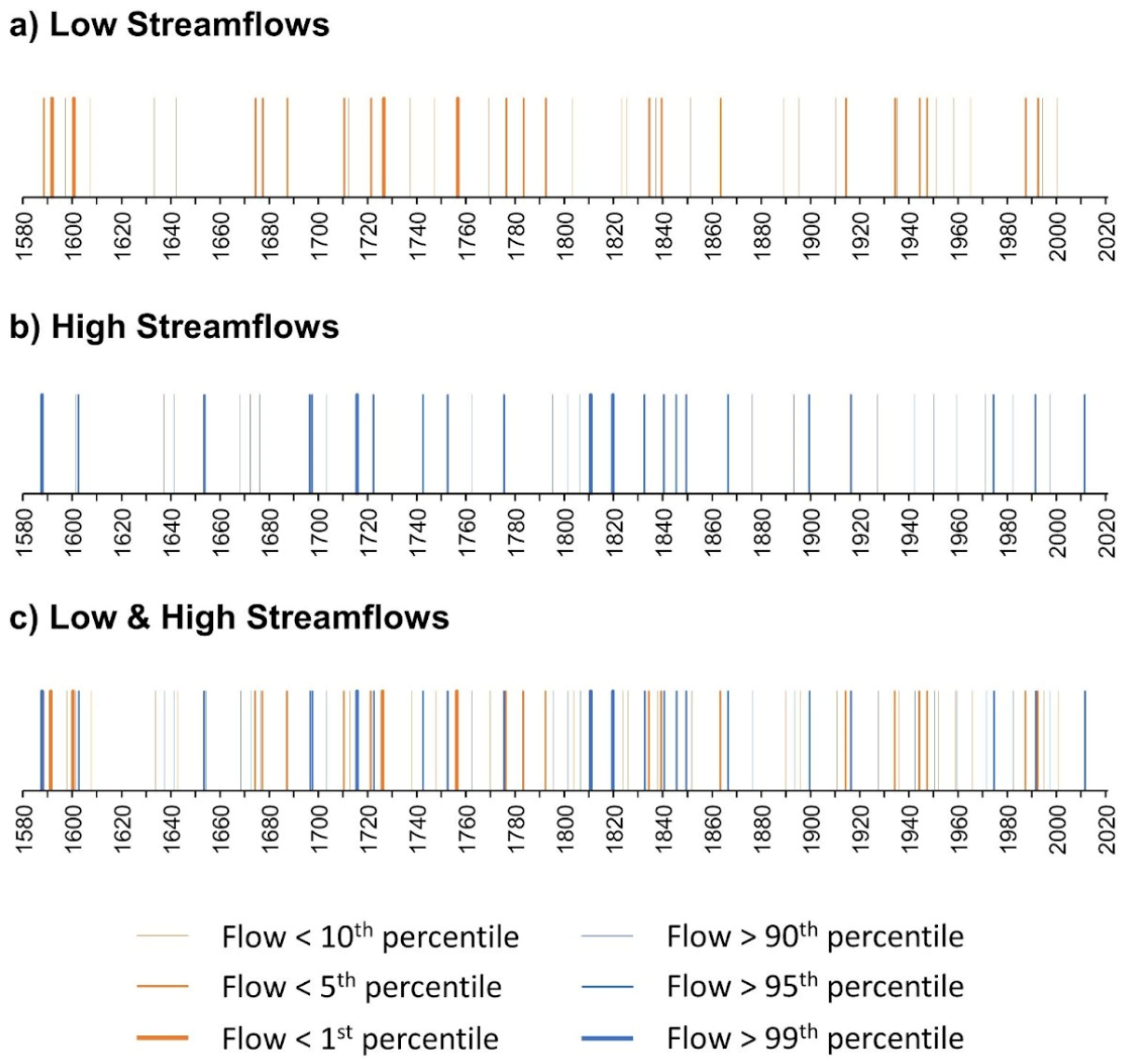

Figure 12. Low and high reconstructed average August streamflows based on percentile rankings.

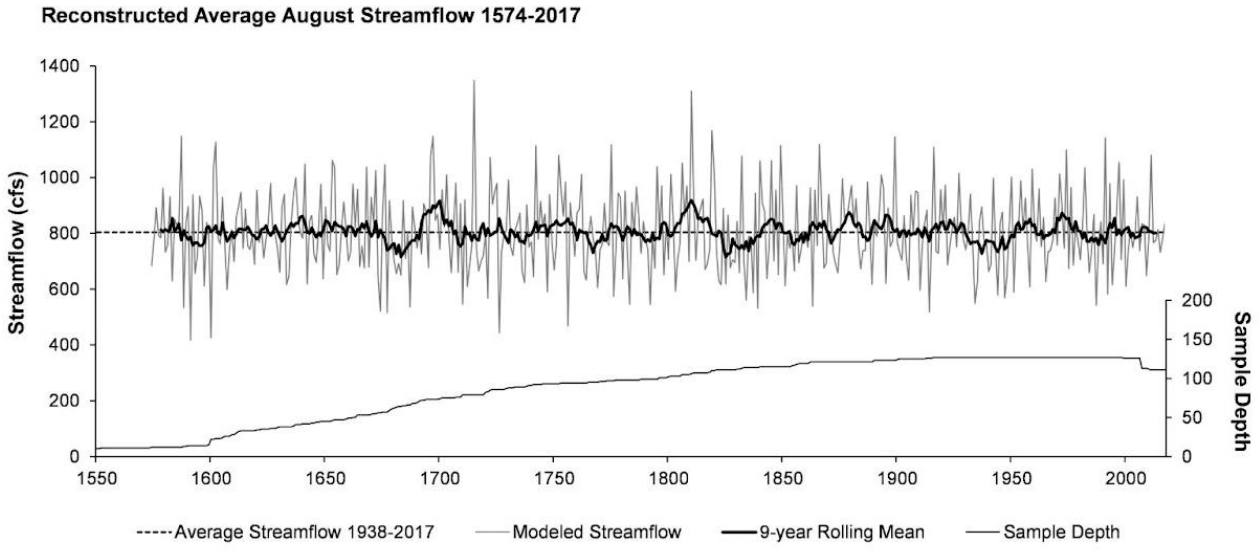

Figure 13. Reconstructed average August Streamflow 1574-2017. The dashed horizontal line indicates the average observed flow of the instrumental data from 1938-2017 (804 cfs). Reconstructed values were plotted with a 9-year rolling mean (bold line) to emphasize trends. The sample depth, or number of cores contributing to each year, is indicated on the secondary axis.